AD-A105 115 DAYTON UNIV OH RESEARCH INST F/G 21/2
ADVANCED COMBUSTION/PLUME DIAGNOSTICS.(U)
JUL 81 J D EVERSOLE F04611-77-C-0042
UNCLASSIFIED UDR-TR-81-01 AFRPL-TR-81-09 NL

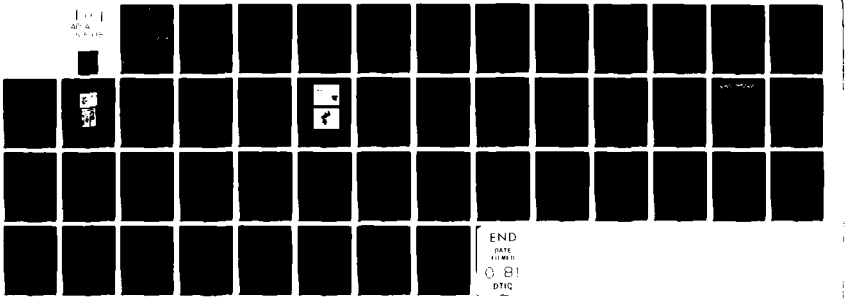

END
DATE FILMED
0 81
DTIC

(2) LEVEL II

AFRPL-TR-81-09 UDR-TR-81-01

AD A105115

ADVANCED COMBUSTION/PLUME DIAGNOSTICS

J. D. EVERSOLE
University of Dayton
Research Institute
Dayton, Ohio 45469

July 1981

Final Report

Approved for Public Release;
Distribution Unlimited

Prepared for:

Air Force Rocket Propulsion Laboratory
Director of Science and Technology
Air Force Systems Command
Edwards Air Force Base, California 93523

NOTICE

"When U. S. Government drawings, specifications, or other data are used for any purpose other than a definitely related government procurement operation, the Government thereby incurs no responsibility nor any obligation whatsoever, and the fact that the Government may have formulated, furnished, or in any other way supplied the said drawings, specifications or other data, is not to be regarded by implication or otherwise, or in any manner licensing the holder or any other person or corporation, or conveying any rights or permission to manufacture, use, or sell any patented invention that may in any way be related thereto."

This report was submitted by the University of Dayton Research Institute, Dayton, OH 45469 under Contract Number F04611-77-C-0042, Job Order Number 999300UC with the Air Force Rocket Propulsion Laboratory, Edwards Air Force Base, CA 93523. The report includes work done from 1 October 1978 to 30 September 1980. The research was performed at the Air Force Rocket Propulsion Laboratory, Edwards Air Force Base, California. The principal investigator was Dr. Jay D. Eversole. Project Manager was Dr. Lawrence P. Quinn and the Task Manager was Dr. David M. Mann. The computer programming was provided by Patrick C. Molloy. Technical assistance was supplied by Ranney G. Adams.

This technical report is approved for release and distribution in accordance with the distribution statement on the cover and on the DD Form 1473.

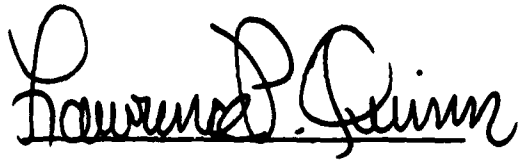

LAWRENCE P. QUINN

FOR THE COMMANDER

JAMES T. EDWARDS

UNCLASSIFIED

SECURITY CLASSIFICATION OF THIS PAGE (When Data Entered)

REPORT DOCUMENTATION PAGE	READ INSTRUCTIONS BEFORE COMPLETING FORM
1. REPORT NUMBER: AFRPL-TR-81-09	2. GOVT ACCESSION NO.: AD-A105 115
3. RECIPIENT'S CATALOG NUMBER:	
4. TITLE (and Subtitle): Advanced Combustion/Plume Diagnostics	5. TYPE OF REPORT & PERIOD COVERED: Final Report, 1 [illegible]-30 [illegible]
6. PERFORMING ORG. REPORT NUMBER: UDR-TR-81-01	
7. AUTHOR(s): Dr. J. D. Eversole	8. CONTRACT OR GRANT NUMBER(s): F04611-77-C-0042
9. PERFORMING ORGANIZATION NAME AND ADDRESS: University of Dayton, Research Institute, Dayton, OH 45469	10. PROGRAM ELEMENT, PROJECT, TASK AREA & WORK UNIT NUMBERS: 61102F 2308M2
11. CONTROLLING OFFICE NAME AND ADDRESS: Air Force Rocket Propulsion Laboratory/XRX, Edwards AFB, CA 93523	12. REPORT DATE: July 1981
	13. NUMBER OF PAGES: 43
14. MONITORING AGENCY NAME & ADDRESS (if different from Controlling Office)	15. SECURITY CLASS. (of this report): Unclassified
	15a. DECLASSIFICATION/DOWNGRADING SCHEDULE

16. DISTRIBUTION STATEMENT (of this Report)

Approved for Public Release, Distribution Unlimited.

17. DISTRIBUTION STATEMENT (of the abstract entered in Block 20, if different from Report)

Approved for Public Release, Distribution Unlimited.

18. SUPPLEMENTARY NOTES

19. KEY WORDS (Continue on reverse side if necessary and identify by block number)

Plume
Diagnostic
Two-Phase Flow
Particles
Blackbody Emission
Infrared Radiation
Infrared Emission

20. ABSTRACT (Continue on reverse side if necessary and identify by block number)

The procedures and some results of an experimental program to record and analyze the thermal radiation from particles suspended in a gaseous flow (two-phase flow) are presented in this report. Carbon particles were added to a nitrogen gas stream at 800-900 K flowing at approximately 50 m/s. Thermal radiation from these particles was observed and recorded using a scanning monochromator for the wavelength range of 1.0 to 5.5 μm. These spectra were

DD FORM 1 JAN 73 1473 EDITION OF 1 NOV 65 IS OBSOLETE

UNCLASSIFIED

SECURITY CLASSIFICATION OF THIS PAGE (When Data Entered)

20. ABSTRACT (Continued)

corrected for instrument response and are compared to theoretical calculations which predict the infrared emission from small particles. Since these predictive calculations depend on the particle size parameter, different techniques were used to obtain the average particle size in the two-phase flow.

-- 1 - AD NUMBER: B050917L
-- 2 - FIELDS AND GROUPS: 21/8.2, 20/6, 21/2, 14/2
-- 3 - ENTRY CLASSIFICATION: UNCLASSIFIED
-- 5 - CORPORATE AUTHOR: DAYTON UNIV OH RESEARCH INST
-- 6 - UNCLASSIFIED TITLE: ADVANCED COMBUSTION/PLUME DIAGNOSTICS.
-- 8 - TITLE CLASSIFICATION: UNCLASSIFIED
-- 9 - DESCRIPTIVE NOTE: INTERIM REPT. 15 MAR 79-15 JAN 80,
--10 - PERSONAL AUTHORS: EVERSOLE, J. D.
--11 - REPORT DATE: AUG , 1980
--12 - PAGINATION: 27P
--14 - REPORT NUMBER: UDR-TR-80-13
--15 - CONTRACT NUMBER: F04611-77-C-0042
--16 - PROJECT NUMBER: 2308, 9993
--17 - TASK NUMBER: M2, 00
--18 - MONITOR ACRONYM: AFRPL
--19 - MONITOR SERIES: TR-80-14
--20 - REPORT CLASSIFICATION: UNCLASSIFIED
--21 - SUPPLEMENTARY NOTE: SEE ALSO REPT. NO. AFRPL-TR-79-32, AD-B040 049L.
--22 - LIMITATIONS (ALPHA): DISTRIBUTION LIMITED TO U.S. GOV'T. AGENCIES ONLY; TEST AND EVALUATION; APR 80. OTHER REQUESTS FOR THIS DOCUMENT MUST BE REFERRED TO DIRECTOR, AIR FORCE ROCKET PROPULSION LAB., ATTN: TSPR(STINFO), EDWARDS AFB, CA 93523.
--23 - DESCRIPTORS: *ROCKET EXHAUST, *SOLID ROCKET PROPELLANTS, *EXHAUST PLUMES, TWO PHASE FLOW, SIMULATORS, DIAGNOSIS(GENERAL), EXPERIMENTAL DESIGN, THERMAL RADIATION, EMISSION SPECTRA, PARTICLE SIZE, REFRACTIVE INDEX, CARBON, PARTICULATES, COMBUSTION, INFRARED SPECTRA, MIE SCATTERING, BLACKBODY RADIATION, DATA REDUCTION
--24 - DESCRIPTOR CLASSIFICATION: UNCLASSIFIED
--25 - IDENTIFIERS: PE61102F, PE62101F, WUAFRPL9993007C
--26 - IDENTIFIER CLASSIFICATION: UNCLASSIFIED
--27 - ABSTRACT: AN EXPERIMENTAL LABORATORY PROGRAM HAS BEEN INITIATED AT THE AIR FORCE ROCKET PROPULSION LABORATORY TO INVESTIGATE AND DEVELOP NEW DIAGNOSTIC TECHNIQUES FOR SOLID-FUELED ROCKET EXHAUSTS (PLUMES). THE EXPERIMENTS CENTER AROUND A GAS/PARTICLE ('TWO PHASE') FLOW APPARATUS DESIGNED TO SIMULATE THE ESSENTIAL FEATURES OF A ROCKET PLUME. CURRENTLY TWO EXPERIMENTS ARE BEING DEVELOPED SIMULTANEOUSLY. THE MAIN PART OF THE PROGRAM CONSISTS OF EVALUATING [illegible] DIAGNOSTIC TECHNIQUES APPLICABLE TO ROCKET PLUMES. ANOTHER EFFORT HAS BEEN MADE TO MEASURE THE THERMAL RADIATION SIMILAR TO THAT FOUND IN ROCKET PLUMES. VERY LITTLE DATA HAVE BEEN AVAILABLE ON THE THERMAL RADIATION PROPERTIES OF SMALL PARTICLES, AND THERE IS SOME SPECULATION AS TO PRECISELY WHAT THE SHAPE OF THE EMISSION SPECTRUM SHOULD BE. THE GREAT ADVANTAGE OF THIS APPROACH OVER TYPICAL COMBUSTION FLOWS IS ITS CONTROL OF THE VARIOUS PARAMETERS.

[illegible] PARTICLE SIZE, PARTICLE COMPOSITION, TEMPERATURE, ETC. PRELIMINARY DATA HAVE BEEN COLLECTED FROM CARBON PARTICLES AT [illegible]. THESE DATA ARE COMPARED WITH TWO THEORETICAL [illegible] BUT THE RESULTS ARE NOT YET CONCLUSIVE. MORE DATA WILL BE [illegible] IN THE NEAR FUTURE AT HIGHER TEMPERATURES, WITH DIFFERENT PARTICLE SIZES, AND WITH ALUMINUM OXIDE PARTICLES AS WELL AS CARBON.
--28 - ABSTRACT CLASSIFICATION: UNCLASSIFIED
--29 - INITIAL INVENTORY: 2
--33 - LIMITATION CODES: 3
--35 - SOURCE CODE: 125400
--36 - [illegible]
--40 - [illegible] 3901
--41 - TYPE CODE: [illegible]

TABLE OF CONTENTS

LIST OF ILLUSTRATIONS

LIST OF ILLUSTRATIONS (Continued)

INTRODUCTION

The subject of thermal radiation from, or emissivity of, micrometer-sized particulate matter is of general interest, but the studies of this radiation have met with difficulty in obtaining experimental data with unambiguous interpretation. Most situations in which particles are generated at high temperatures, such as rocket or engine exhausts, are quite complex; the observed radiation spectra are not sufficiently structured to specify the host of variables which enter an a priori calculation of particle emission. Typical emission parameters which may be difficult to measure in combustive flows producing or including particles would be: (a) particle size distribution, (b) particle composition distribution, (c) particle structure and shape distribution, (d) corresponding bulk indices of refraction, (e) spatial and temporal changes in these distributions and also in temperature, and (f) other molecular (gas) species which may emit continuous or quasi-continuous bands of infrared radiation.

Because there are so many variables, the general radiation characteristics of particulate matter have not been verified experimentally. In addition, there are fundamental theoretical questions still unanswered. What theoretical model should be used in predicting particle radiation?[1] What is the size limitation of a valid "classical" description?[2] What is the effect of exceeding that size limitation? This report presents results of an experiment in which the variables are either measured or minimized and compares the observed spectra with calculations based on Mie Theory, Planck blackbody radiation, and bulk values of the index of refraction.

---

1. McGregor, W. K., "On the Radiation from Small Particles," J. Quant. Spectropscopy Radiation Transfer 19, 659 (1978).

2. Kawabata, A. and Kubo, R. J., Phys. Soc. Japan 21, 1765 (1966).

SECTION 1
OBJECTIVES

The principal objective of this program was to explore possibilities for more refined, nonobtrusive diagnostic techniques applicable to combustive flows such as a solid propellant rocket motor plume. One of the areas investigated was the thermal emission from two-phase flows. The experiment was designed to exert as much control as possible over the various parameters which affect the thermal radiation spectra emitted by suspended particulate material. Therefore, the primary objective was to measure accurately the thermal radiation from a well-characterized two-phase flow and then, if possible, to use these data to refine theoretical formulations for predicting infrared emission from such flows.

SECTION 2
EXPERIMENTAL APPROACH

2.1 TWO-PHASE FLOW APPARATUS

The experimental approach is in principle simple and straightforward. The greatest difficulty is in constructing a gas and particle, or two-phase, flow apparatus with a constant flow velocity in which the composition, size, temperature, and particle density are controlled. Figure 1 is a schematic diagram of the two-phase flow apparatus which has evolved. The basic components of the system are a powder hopper with an auger feed, a particle suspension tank, and a gas heater. The particle feeder is a commercial unit which can hold 30 ℓ of powdered material. The feeder transports the particles with a variable speed auger screw. A gas heater is constructed out of roughly 4 m of 12.5-mm diameter stainless steel tubing bent into a coil. Short pieces of smaller diameter stainless steel tubing were inserted before the coil was formed to improve heat transfer to the gas by breaking up laminar flow and providing greater surface area. Cables to an arc welder capable of providing up to 200 A are connected to either side of the coil which is isolated from electrical ground by ceramic feed-throughs. The coil is then enclosed in an aluminum box which is thermally insulated with zirconium oxide. When the tube is electrically heated, the N_2 gas flowing through the tubing can reach temperatures in excess of 1,300 K. The main gas stream is introduced into the system at about 180 kPa (25 psi). A smaller N_2 gas flow is maintained through the holding-suspension tank to transport the particles through the exit nozzle. The nozzle throat was 10 mm in diameter, and pressure behind it was principally due to the carrier gas flow. This overpressure was typically held between 10 and 20 kPa, since the particle feeder was not originally designed to hold pressure. Calculations based on this pressure and measurements made with anemometers indicate normal flow velocities of 50 m/s at the exit plane.

2.2 OPTICAL SYSTEM

Once a flow of heated particles is achieved, it is very straightforward to set up instrumentation for the detection and spectral analysis of infrared

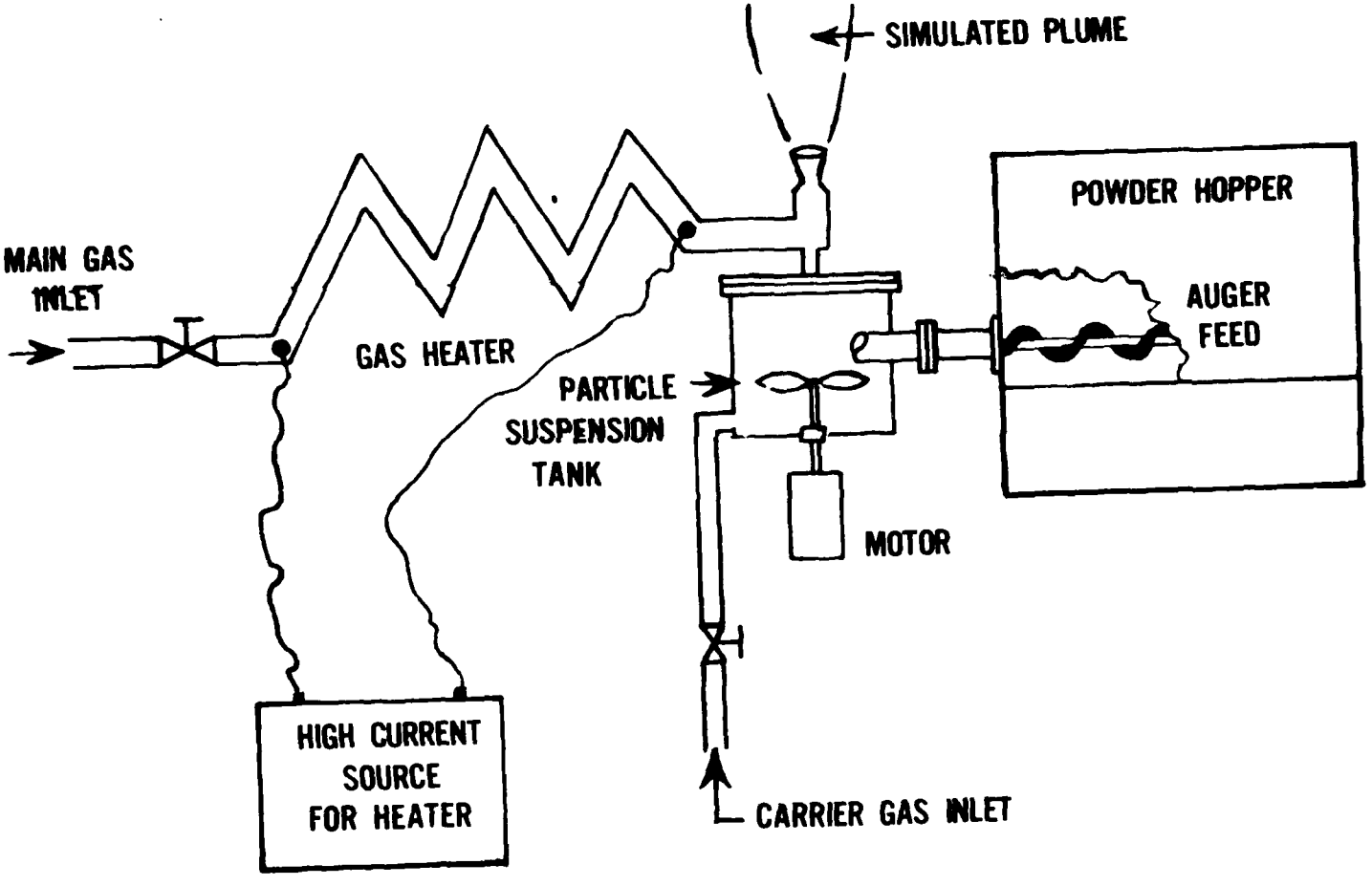

Figure 1. Two-Phase (Gas/Particle) Flow Generator.

radiation. Since nitrogen gas does not have infrared-active modes, any radiation observed must be due to the particles. The optical path consists of a collecting lens which focuses the emitted radiation onto the entrance slit of a 1/4-m scanning monochromator, and a curved mirror which focuses the radiation from the exit slit onto an InSb detector. A chopping wheel is placed in front of the monochromator. Output of the detector and preamplifier is measured with a lock-in amplifier synchronized to the chopping frequency.

Figure 2 shows photographs of the apparatus. In Figure 2(a), the particle feeder is located on the left. On the right is an instrument rack containing the monochromator and associated electronics. In the lower middle section of the picture is the gas heating coil with the insulation box removed. Behind the coil is the suspension-holding tank with the exit nozzle on top. Figure 2(b) is a different perspective of the same apparatus, showing the holding-suspension tank in the lower middle. The heating coil is on the right, with the insulation box now in place.

In addition to the infrared radiation spectral measurement, other optical systems monitor relative changes in particle density in the flow stream. Scattering of HeNe laser light by the particles is detected by a photomultiplier tube and lens, and the transmitted beam is monitored by a photodiode. Figure 3 is a schematic diagram of the optical arrangement for making all the various measurements, although they were generally not carried out simultaneously. All the optical diagnostic measurements are centered at a height of 10 mm (1 nozzle diameter) from the nozzle exit plane. With the laser unfocused, photon correlation spectroscopy techniques could be used, and with a focused beam, discrete particles could be counted. A blackbody calibration source is used to determine the absolute instrument response of the monochromator and detector (Fig. 3). Due to the effects of second order diffraction, it is necessary to use cutoff filters and measure the spectrum in three wavelength segments: 1.5 to 2.4 μm, 2.4 to 3.6 μm, and 3.6 to 5.5 μm. The long wavelength cutoff is due to the cooled InSb detector response.

The laser light scattering signal from the photomultiplier tube is amplified and recorded on FM tape with a frequency response of 0-10 kHz. For the photon correlation spectroscopy measurements the signal is played back into an analog-to-digital fast Fourier transform computer (SD-360), and the

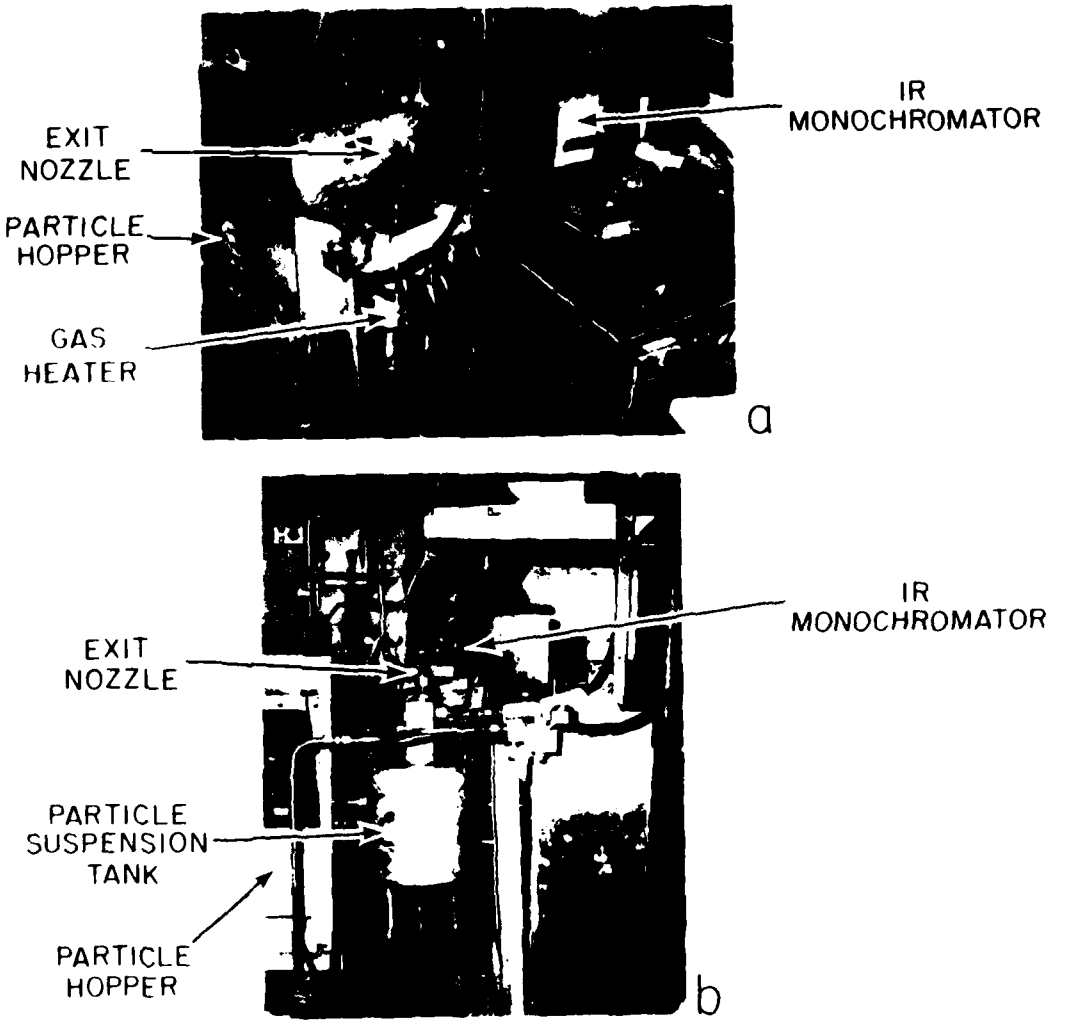

Figure 2(a and b). Photographs from Different Perspectives of the Two-Phase Flow Generator and the Infrared Radiation Detection Instrumentation. (a) Detection Instrumentation is right with Flow Generator left. (b) Detection Instrumentation is behind Flow Apparatus in foreground.

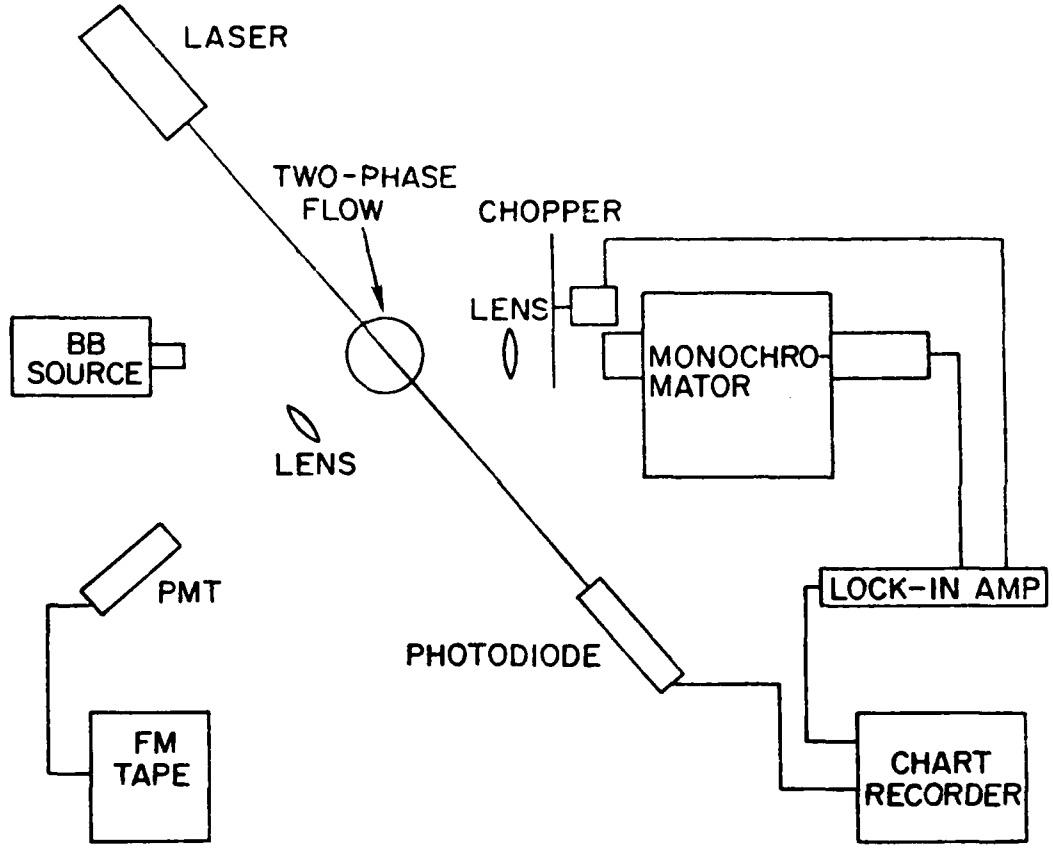

Figure 3. Schematic Diagram of Optical Measurement Geometry Looking Along the Axis of the Two-Phase Flow.

results output to an x-y plotter. For the discrete particle detection the FM tape is speed-scaled down and played back into an optical chart recorder. The laser attenuation is monitored by a photodiode/op-amp detector input directly to a strip chart recorder.

2.3 PARTICULATE MATERIAL

Only one type of particulate material has been used in the flow apparatus - a pure carbon powder available commercially.[3] The size distribution of this material as single particles was measured on a scanning electron microscope, as shown in Figure 4. Nearly all the powder has an initial size of less than 0.5 μm in diameter. There was the question of whether this remains an accurate description of particle sizes in the gas flow since agglomeration could take place during transport and mixing with the nitrogen. Samples were taken from the two-phase flow, by passing a clean tantalum surface through the flow stream. These tantalum discs were examined with a scanning electron microscope, and while individual carbon spheres on the order of 0.5 μm were in evidence, there were also a significant number of large agglomerated particles up to 15 μm in diameter. Figure 5 (a and b) shows representative photomicrographs taken with the scanning electron microscope.

Some indication of the degree of this agglomeration was needed, since the spectral data would be a function of the particle size distribution. The simplest technique for determining average size is to measure simultaneously laser beam attenuation and scattering. By focusing the laser beam to a small enough diameter, it is possible to use a photomultiplier tube to detect scattered laser light from a single particle rather than a group of particles. By counting the average number of discrete particles under normal flow conditions and calculating the scattering volume, the density of particles was directly measured to be $\sim 5 \times 10^4/cm^3$. This number can be coupled with the attenuation

---

3. Thermax Powder from R. T. Vanderbilt Co. Inc., 6273 E. Slauson, Los Angeles, CA.

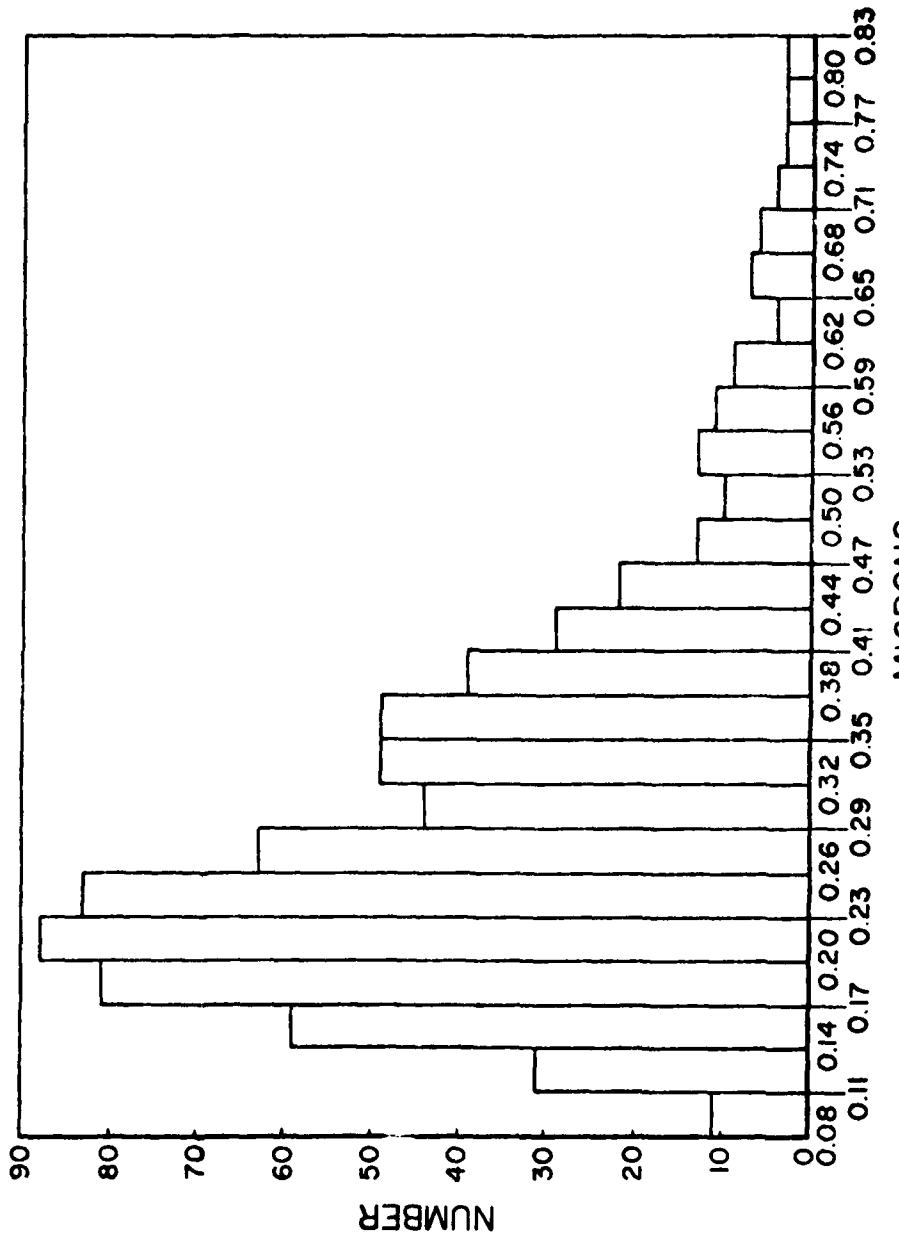

Figure 4. Distribution of Single Carbon Particle Diameters Used in the Two-Phase Flow.

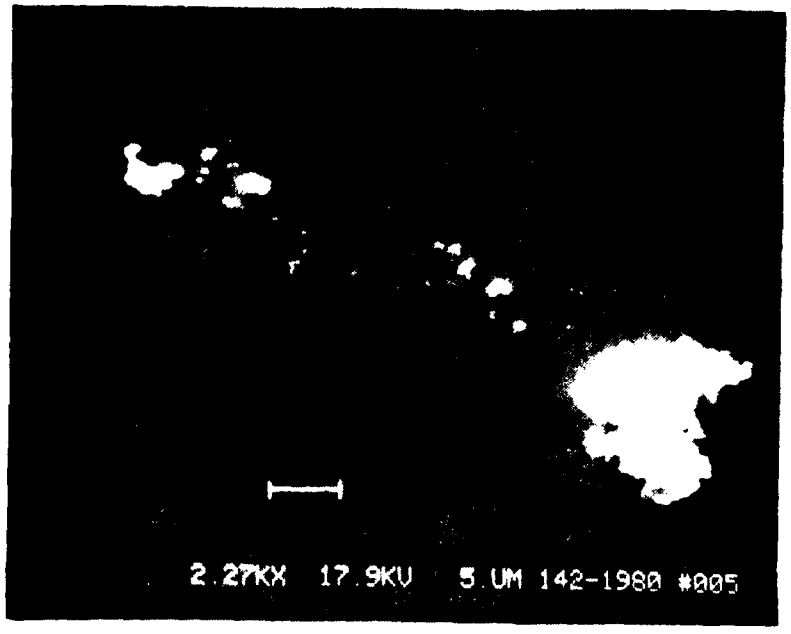

A

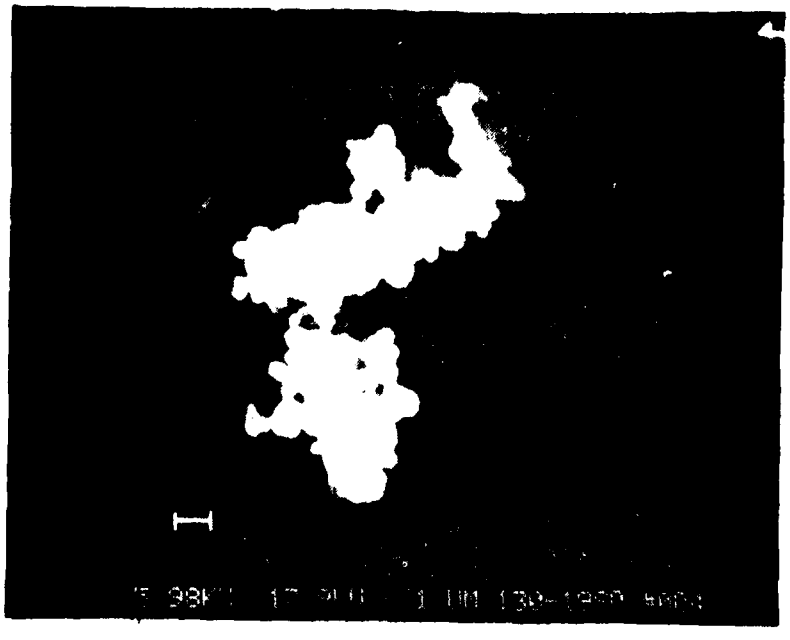

B

Figure 5(a and b). Photographs from Electron Microscope of Particulate Samples Collected in the Two-Phase Flow at Low Flow Rates. In 5a the scale bar is 5 μm. In 5b the scale bar is 1 μm and the individual particles can be seen as 0.5 μm or less in diameter. The question is whether such agglomerates are present in the flow.

of the laser beam as it passes through the particle flow by the equation:

$$-\ln(I/I_o) = \bar{\rho} \cdot \bar{\sigma} \cdot L \tag{1}$$

where I_o and I are the initial and attenuated laser intensities, L is the pathlength through the two-phase flow, and $\bar{\rho}$ and $\bar{\sigma}$ are the average density and extinction cross section for the particles. Average attenuation of the laser is 2.5 ∓ 0.5 percent. Using $5 \times 10^4/cm^3$ for $\bar{\rho}$, $\bar{\sigma}$ can be calculated to provide an average particle diameter of 2.6 μm.

A more sophisticated technique was also employed to obtain an average particle size. By recording the Rayleigh (elastic) scattering from a group or population of particles, correlation spectroscopy can be used to determine their diffusion rate. Detailed explanations of this technique can be found elsewhere.[4-6] Only a concise outline is given here. Consider the scattered electric field from a single particle. From Figure 6, $\vec{k}_o$ is the initial light wave vector and $\vec{k}_s$ the wave scattered from the j^{th} particle. The electric field due to scattering from this particle can be written as

$$\vec{E}_j = \vec{E}_o \exp\ i[\vec{k}_o \cdot \vec{r}_j + \vec{k}_s \cdot (\vec{R}_o - \vec{r}_j) - \omega t] \tag{2}$$

where $\vec{r}_j$ is the position vector from the origin to the j^{th} particle, and $\vec{R}_o$ is the position vector to the detector. A simplification is made by defining a scattering wave vector, $\vec{K}$, by

$$|\vec{K}| = \vec{k}_o - \vec{k}_s \tag{3}$$

---

4. Penner, S. S., Bernard, J. M., and Jerskey, T., Acta Astronautica 3, 93 (1976).

5. Clark, N. A., Lunacek, J. H., and Bendek, G. B., Am. J. Phys 38, 575 (1970).

6. Schaefer, D. W. and Berne, B. J., Phys. Rev. Letters 28, 475 (1972).

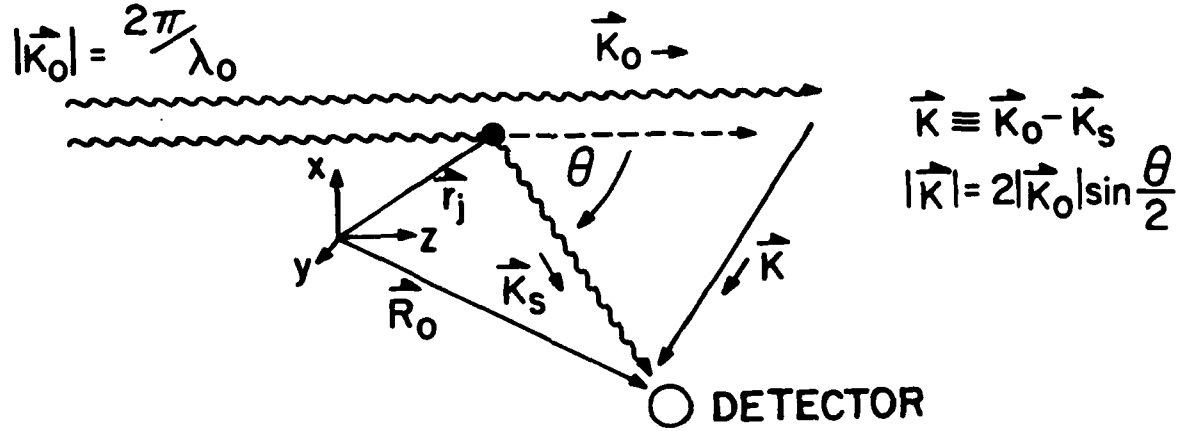

Figure 6. Schematic Diagram of Elastic Scattering of Laser Light of Wavelength λ_o from Particle Located at Position $\vec{r}_j$ to Detector Located at $\vec{R}_o$.

From Figure 6 it can be shown that

$$|\vec{K}| = 2\, k_o \sin(\theta/2) \tag{4}$$

Substituting Eq. (3) into Eq. (2) yields

$$\vec{E}_j = \vec{E}_s \exp\{i\,(\vec{K} \cdot \vec{r}_j)\} \tag{5}$$

where $\vec{E}_s = \vec{E}_o \exp\{i(\vec{k}_s \cdot \vec{R}_o - \omega t)\}$. The total electric field at the detector is merely the sum of the scattering fields from N individual particles, or,

$$\vec{E}_T = \sum_{j=i}^{N} \vec{E}_j = \vec{E}_s \sum_{j=i}^{N} \exp\left[i(\vec{K} \cdot \vec{r}_j)\right] \tag{6}$$

A useful expression would link the electric field to the power spectrum of the intensity of light at the detector. A connection is found in the Wiener-Khinchine theorem which states that the power spectrum is the Fourier transform of the autocorrelation function.

The autocorrelation function measures the degree of coherence a function has with a copy of itself shifted in time by an amount τ. If "n" is a particle at time t, and "m" a particle at time $t + \tau$, the field correlation function is given by

$$\int E_T(t)\, E_T^*(t+\tau)\,dt = \sum_{n=1}^{N} \sum_{m=1}^{N} \int E_s E_s \exp\left\{i\left[\vec{K} \cdot \vec{r}_n(t) - r_m(t+\tau)\right]\right\} dt \tag{7}$$

Because the time dependence is evident only in the change in particle position, the integral can be changed from a time-dependent to a position-dependent integral, and Eq. (7) rewritten as

$$\sum_{n=1}^{N}\sum_{m=1}^{N}\int E_s\, E_s \exp\left\{i\vec{K}\cdot\left[\vec{r}_n(t)-r_m(t+\tau)\right]\right\} dt \qquad (8)$$

$$= NE_s^2 \overline{\sum_j \exp(i\vec{K}\cdot\Delta\vec{r}_j}$$

where $\Delta\vec{r}_j = \vec{r}_j(t) - \vec{r}_j(t+\tau)$. The ensemble average over $\Delta\vec{r}_j$ is given by

$$\overline{\sum_j \exp\,(i\vec{K}\cdot\Delta\vec{r}_j)} = \int_{-\infty}^{\infty} f(\Delta\vec{r},\tau)\exp\left[i(\vec{K}\cdot\Delta\vec{r}_j)\right] d\Delta\vec{r} \qquad (9)$$

where $f(\Delta\vec{r},\tau)$ is the conditional probability that a particle moves $\Delta\vec{r}$ in a time period τ. In the model, the only change in position through time τ is due to random Brownian motion; thus the probability of a particle moving $\Delta\vec{r}$ in a time τ is given by[7]

$$f(\Delta\vec{r},\tau) = (4\pi D\tau)^{-1/2}\exp(-|\Delta\vec{r}|^2/4D\tau) \qquad (10)$$

Where D is the diffusion coefficient for Stoke's flow and where molecular mean free path is small compared to particle size,

$$D = kT/3\pi\mu d \qquad (11)$$

where

k is the Boltzmann constant

T is the temperature

μ is the coefficient of viscosity

d is the average particle diameter.

---

7. Present, R. D. Kinetic Theory of Gases (McGraw-Hill, New York, 1958), p. 158 .

Combining Eq's. (7) through (11) and integrating gives the field correlation function as

$$\int E(t)E^*(t+\tau)dt = NE_s^2 \exp(-K^2D\tau) \tag{12}$$

Using the Weiner-Khinchine theorem, the Fourier transform of Eq. (12) will provide an expression for the power spectrum,

$$P_s(\omega) = \frac{1}{2\pi}\int_{-\infty}^{\infty} NE_s^2 \exp(-K^2D\tau)\exp(-i\omega\tau)d\tau = \frac{NE_s^2K^2D/\pi}{(K^2D)^2 + (\omega)^2} \tag{13}$$

This expression for the power spectrum is conveniently in the form of a Lorentzian curve given by

$$Y = \frac{C}{(HW)^2 + X^2} \tag{14}$$

where HW is the "halfwidth" of the curve. So far the derivation has dealt with the field correlation function for simplicity. However, the measurable quantity is the scattered light intensity, not the field strength. Hence, the field correlation function (Eq. 12) is squared to obtain the intensity correlation function. Since squaring an exponential function simply multiplies the argument by a factor of two, the form of the power spectrum is preserved (neglecting dc terms). In going from the field to the intensity, simply substitute $2K^2D$ for K^2D in Eq. (13). This implies that the intensity power spectrum is twice as wide as the field power spectrum. This derivation makes the necessary theoretical connection between the intensity power spectrum and physical parameters. Operationally, the light intensity power spectrum is obtained by taking the absolute value squared of the Fourier transform of the measured scattered light intensity as a function of time. Therefore, the

power spectrum of the scattered light intensity as a function of time yields a Lorentzian curve with a halfwidth given by:

$$HW = 2K^2D = \frac{4k_o^2 \sin^2(\theta/2)kT}{\mu d\pi^2} \quad \text{rad/sec} \qquad (15)$$

Figure 7 is a graph of the scattered light signal (time series) from the photomultiplier, and the corresponding power spectrum from which the halfwidth of 50 Hz yields an average diameter of 3.4 μm through Eq. (15). This technique was perfected and calibrated by first performing a similar measurement on polystyrene latex spheres suspended in water. Since the latex spheres were commercially prepared and measured to be a certain diameter (0.312μm in this case), the degree of absolute error in the measurement could be assessed and was found to be ~7 percent. However, all the usable data obtained on the two-phase flow apparatus were taken at low flow rates. Velocities on the order of 2 cm/s were indicated from the widths of single particle-scattering pulses. When normal flow conditions were established (~50 m/s), a large spike centered at 0 Hz in the power spectrum buried the data. Therefore, utilization of these data requires the assumption that the size distribution is independent of the flow conditions. The indicated particle size of 3.4 μm is therefore considered to be in reasonably good agreement with the previous measurement of 2.6 μm, taken under normal flow conditions independently.

Some assessment of the degree of agglomeration is achieved on the basis of these in situ measurements and calculations. However, there is still a certain degree of arbitrariness in specifying the particle size distribution, since the measurements reflect only on some sort of "mean" size. In the absence of more information about the particle size distribution in the flow, the analysis of the data presumed a standard two-parameter, log-normal distribution. One parameter is obtained from the particle size measurements, which are equated with the geometric mean of the distribution since they are based on light scattering and extinction, and therefore weigh the results by the particle cross-section (proportional to d^2 in this case where $d \sim \lambda$). The second parameter is derived from the hypothesis that the most numerous

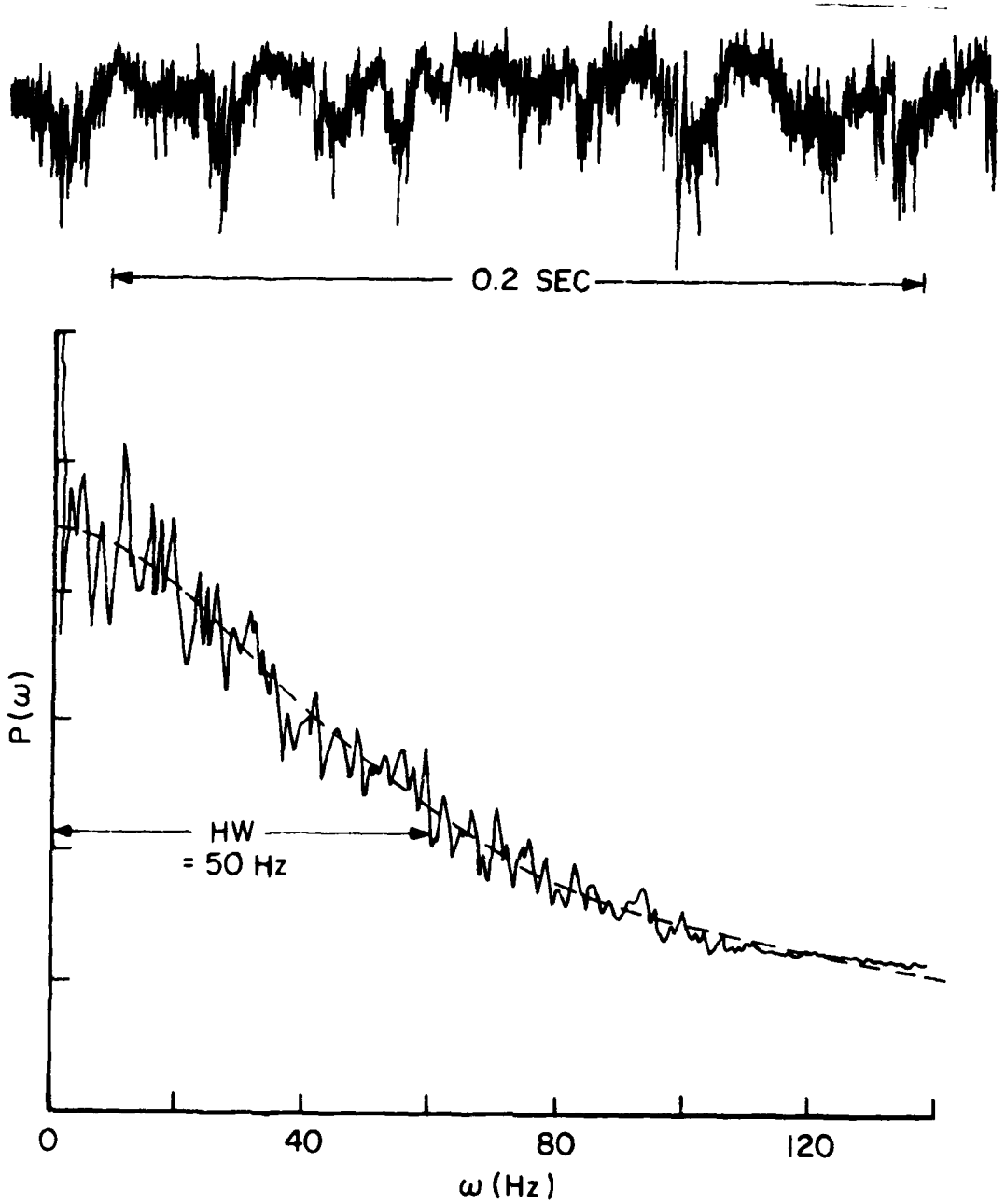

Figure 7. Scattered Laser Light Signal from Particles and Corresponding Power Spectrum Showing Lorentzian Line Shape. (The Lorentzian halfwidth implies a mean diameter of 3.4 μm).

particle size distribution mode in the flow is not much greater than in the original distribution (Fig. 4). Due to time constraints, analytical predictions were based on size distributions represented by three size groupings: 0-1 μm, 1-5 μm, and 5-9 μm. Table 1 is a typical example of representative particle sizes for each grouping and their relative number frequencies for a distribution with a geometric mean of 2.0 μm and a mode of 0.5 μm. This distribution might be termed "optimistic" since the mean is smaller than indicated by the size diagnostic measurements. However, as will be discussed later, the resulting calculated spectra are relatively insensitive to this sort of variation in the size distribution.

TABLE I
PARTICLE SIZE DISTRIBUTION

Size (μm)	0.5	3.5	6.5
Relative Number	800	100	5

2.4 DATA HANDLING AND REDUCTION

Infrared emission and laser scattering data are recorded on a strip chart, dual pen recorder along with wavelength event marks. This information is then transcribed to digital form and stored on a computer disc. Manipulation and correction of the data are performed by computer and the corrected output is then graphed by a computer-operated plotter. The data are primarily corrected for the optical system with the same geometric arrangement as for the particle flow. The measured spectrum of the calibration source is then compared to the "known" spectrum of the source generated by computer from the Planck equation:[8]

$$U(\lambda,T) = \frac{2\pi hc^2}{\lambda^5} \quad \frac{1}{\exp(hc/\lambda kT)-1} \quad . \tag{16}$$

8. Reif, F., Fundamentals of Statistical and Thermal Physics (McGraw-Hill, New York, 1965), pp. 378-388.

Differences between the two are due to the response function of optical system and detector. Once the response function was determined, it was stored in the computer for reduction of all subsequent data taken of heated particle flow. Various tests on the entire reduction system indicate that the amount of error introduced by the digitization and computer reduction was held to within 1.0 percent and typically runs about 0.2 percent. Since the signal-to-noise ratio in the particle data runs between five and twenty percent, this error introduced by processing is negligible. As mentioned, the spectrum from 1.5 to 5.5 μm wavelengths had to be taken in three segments with cutoff filters primarily to avoid difficulties with second order diffraction. For the long wavelength region (3.6 to 5.5μm) a different grating was also required. Figures 8, 9, and 10 illustrate the relative instrument response curves for the three wavelength regions respectively. In each case the blackbody calibration source is recorded for a number of different temperatures. These spectra are then divided by the appropriate blackbody (Planck) curve to provide the instrument response curves illustrated. The response curves from the different temperatures are averaged together to improve signal-to-noise ratios before being used to reduce data from the particle flow. Since the radiation from the calibration source is known in absolute intensity (not just relative spectral intensity), it was possible to obtain absolute instrument response. (Note that the vertical scales in Figures 8 through 10 are in millivolts/milliwatts.) In the calibration procedure it was not physically possible to locate the calibration source at the focal volume of the monochromator and collecting lens. Instead, an aperture was placed in the focal volume and the calibration source was located 80 mm behind the aperture. Since the monochromator was operated with 0.5 mm x 20 mm slits and 2:1 imaging, the aperture used for calibration was 0.25 mm x 10 mm. Therefore, the measured spectra in millivolts was divided by the Planck equation (Watts) and multiplied by the solid angle of the radiation times the area of the aperture. It should be noted that the angular dependence has been removed from the common form of Planck's radiation equation (Eq. 16) by integrating the solid angle over a hemisphere. The actual angular dependence is $\cos\theta$ where θ is the angle between the observer and the normal to the radiating surface (calibration source). Hence, the integration results in a factor of π in Eq. (16). However, due to the small aperture used, the

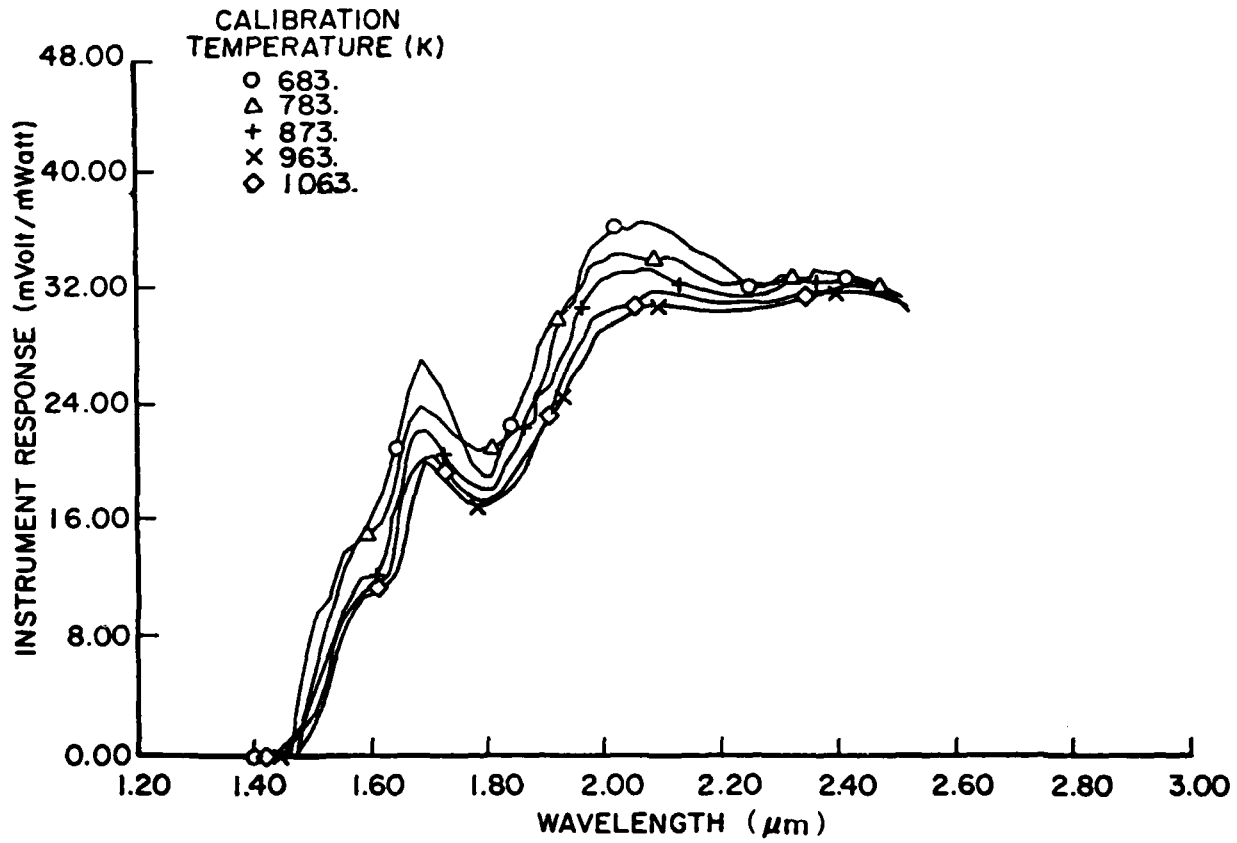

Figure 8. Absolute Instrument Response Curves for the 1.5 to 2.4 μm Spectral Region for Various Calibration Source Temperatures.

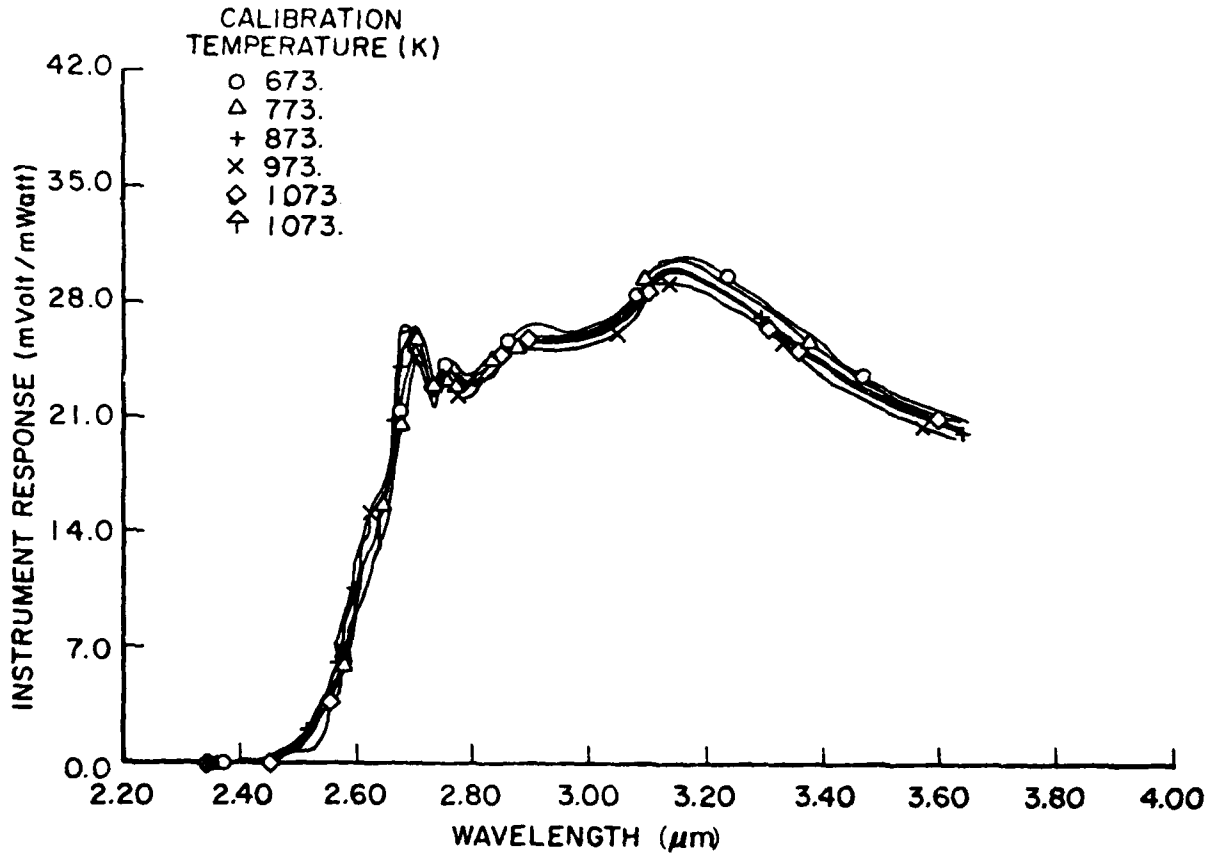

Figure 9. Absolute Instrument Response Curves for the 2.4 to 3.6 μm Spectral Region for Various Calibration Source Temperatures.

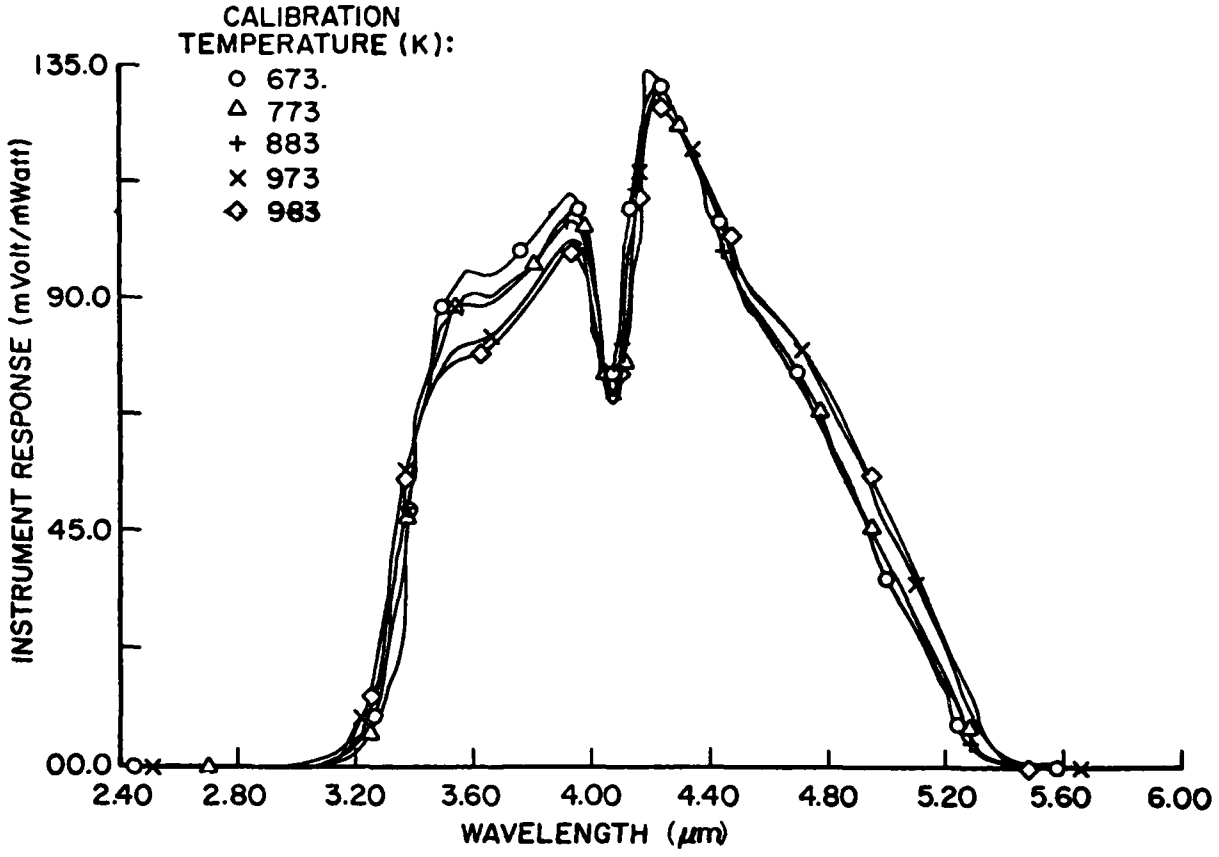

Figure 10. Absolute Instrument Response Curves for the 3.6 to 5.5 μm Spectral Region for Various Calibration Source Temperatures.

cos θ term can be accurately approximated by 1, and therefore it is legitimate to simply multiply by the subtended solid angle rather than make some attempt at integration.

SECTION 3
RESULTS AND ANALYSIS

3.1 PREDICTIVE CALCULATIONS

In order to evaluate the data obtained from thermal emission, it was necessary to compare the data with theory. The most convenient way to do this is to generate calculated spectra using the measured particle size, measured temperature, and established values for the index of refraction. The calculated spectra were then compared to the reduced measurements. Since part of the initial impetus for this experiment was to confirm or refute a novel prediction for particle radiation (discussed in the following paragraphs), the theoretical aspects are presented first.

3.1.1 Modified Planck Equations

From basic physics, the discussion of thermal radiation usually begins with an enclosed cavity whose walls are maintained at a constant temperature so that with a sufficient amount of time the radiation field inside the cavity comes into equilibrium with the walls. This is a well-defined and straightforward problem in equilibrium thermodynamics, and the energy density of the radiation inside the cavity is given by the Planck equation[9]

$$U(\omega,T)d\omega = \frac{\hbar\omega^2 d\omega}{2\pi^3 c^3} \quad \frac{\omega}{\exp(\hbar\omega/2\pi kT) - 1} \tag{17}$$

where the energy per unit volume and unit frequency, U, is a function of the frequency (ω) and temperature (T), h is Planck's constant, k is Boltzmann's constant, and c is the velocity of light. It is fairly common to generalize this problem by considering a small hole or aperture in the cavity through which radiation can pass, and to describe the absorption and emission of an "ideal" object (blackbody) as being represented by the radiation absorption/emission of the aperture. The radiation flux emitted by the cavity

9. Ibid.

through the aperture is obtained from Eq. (17) by including a factor of $c/4$,[10] and can be rewritten in terms of the wavelength, as Eq. (16).

In Eq. (17) the right side has been written as the product of two parts. The first part describes the number of photons per mode (eigenstate in the cavity) and the second part comes from the density or number of modes available in the cavity. A recent paper[11] focused on the degree of arbitrariness with which this density of modes is derived and suggested that it be altered to include the situation in which radiation wavelengths are comparable to cavity dimensions. The modified form of the Planck equation was thus derived and has the following form

$$M_1(\lambda,T,d) = U(\lambda,T)\ \{1 - (\lambda^2/2\pi^2d^2)\} \qquad (18)$$

where M_1 is the new radiance function, U is given in Eq. (16), and d is the cavity diameter. Since data have previously been scarce, it was speculated that this formulation could be applied to particle thermal radiation. For diameters less than one μm, the effect of this new term is very significant. The radiation actually terminates instead of tailing off to wavelengths longer than 5μm.

3.1.2 Mie Theory Calculations

The conventional method of calculating thermal radiation is to multiply the standard Planck equation by an emissivity function. In general, the emissivity is characteristic of the material in question and is a way of accounting for the fact that a given material may absorb or emit more or less strongly in one wavelength region than in another, in comparison to the "ideal" blackbody described by the Planck equation. The emissivity of a material is related to the index of refraction (dielectric constant) of the material and hence is measurable. However, in the situation where the dimensions of the material object are comparable to the wavelengths of interest (as

---

10. Kittell, C., Thermal Physics (Wiley, New York, 1969), p. 256.
11. McGregor, W. K., op. cit.

is the case with thermal radiation from μm-sized particles), geometric optics is no longer applicable, and some attempt must be made to solve the electromagnetic boundary value problems.

The solution to Maxwell's equations for a plane electromagnetic wave impinging on a sphere with a given dielectric constant is generally referred to as Mie Theory, the details of which are discussed elsewhere.[12] Mie Theory provides a method to calculate the total extinction cross section and the total scattering cross section of a sphere as a function of radius, wavelength, and index of refraction. The difference between the amounts of extinction and scattering is by definition the amount of absorption. Therefore, an absorption efficiency factor (Q_{abs} = absorption cross section/ geometric cross section) can be calculated. Thermal radiation of a particle is then obtained by multiplying the efficiency factor (equal to the emissivity via Kirchoff's Law) by the Planck blackbody radiation equation, Eq. (16):

$$M_2(\lambda,T,d,n) = Q_{abs}(\lambda,d,n)\ U(\lambda,T) \qquad (19)$$

where n is the bulk index of refraction. Calculations of Q_{abs} used 1.7 - i 0.80 for the index of refraction for carbon particles.[13] For larger particles (1.0μm diameter and above), Q_{abs} is fairly flat across this wavelength range so that the resulting particle radiation will not be significantly different from the normal Planck radiation spectrum, Eq. (16). However, for smaller particles this is not the case; the Planck radiation curve will be heavily weighted at shorter wavelengths.

3.1.3 Theoretical Predictions

Computer programs have incorporated equations 17 and 18 to provide graphs of the calculated thermal radiation spectra. To illustrate the

---

12. Kerker, M., The Scattering of Light and Other Electromagnetic Radiation (Academic Press, New York, 1969).

13. Pluchino, A. B., Goldberg, S. S., Dowling, J. M., and Randall, C. M., J. Appl. Opt. 19, 3370 (1980).

differences involved, Figure 11 compares three calculated spectra at a temperature of 800 K. The solid curve corresponds to the Planck blackbody radiation law (Eq. 16). The lower dashed curve corresponds to the modified form of the Planck equation (Eq. 18) summed over the particle size distribution shown in Figure 4. To show this spectrum on the same vertical scale, the values had to be multiplied by a factor of 10. The upper dotted curve is calculated using Mie theory (Eq. 19) summed over the same particle size distribution and using an index of refraction of 1.7 - i 0.8. The spectra reflect the interesting features previously discussed in which the modified Planck equation predicts a definite long wavelength cutoff to the radiation, and in which the absorption coefficient from Mie theory emphasizes the shorter wavelengths compared to the longer wavelengths. Both of these effects are dependent on small particle size. It should be expected that, as this parameter is increased, both broken curves will eventually converge to the solid curve since, physically, a transition is being made from a small particle to a macroscopic object for which the Planck equation (Eq. 16) is known to be accurate. Figure 12 illustrates this assertion with graphs of Eq's (16), (18), and (19) again, except that the particle distribution used for Eq's (18) and (19) contains the larger particle sizes shown in Table I at a temperature of 800 K.

To compute the thermal radiation from a size distribution, each particle size is taken separately and the absolute radiation spectrum is calculated for that size. This spectrum is then multiplied by the surface area and the relative number frequency of the particle in the distribution. These separate spectra are then added together for each wavelength value and the total is divided by the total surface area of the distribution. Algebraically, Figures 11 and 12 display the quantity:

$$\frac{\sum_i M_{ki} S_i N_i}{\sum_i S_i N_i} \qquad (20)$$

where M_k is the appropriate radiance function (Eq's 18 or 19), the index, i, refers to the particle size, S is the surface area of the particle, and N is

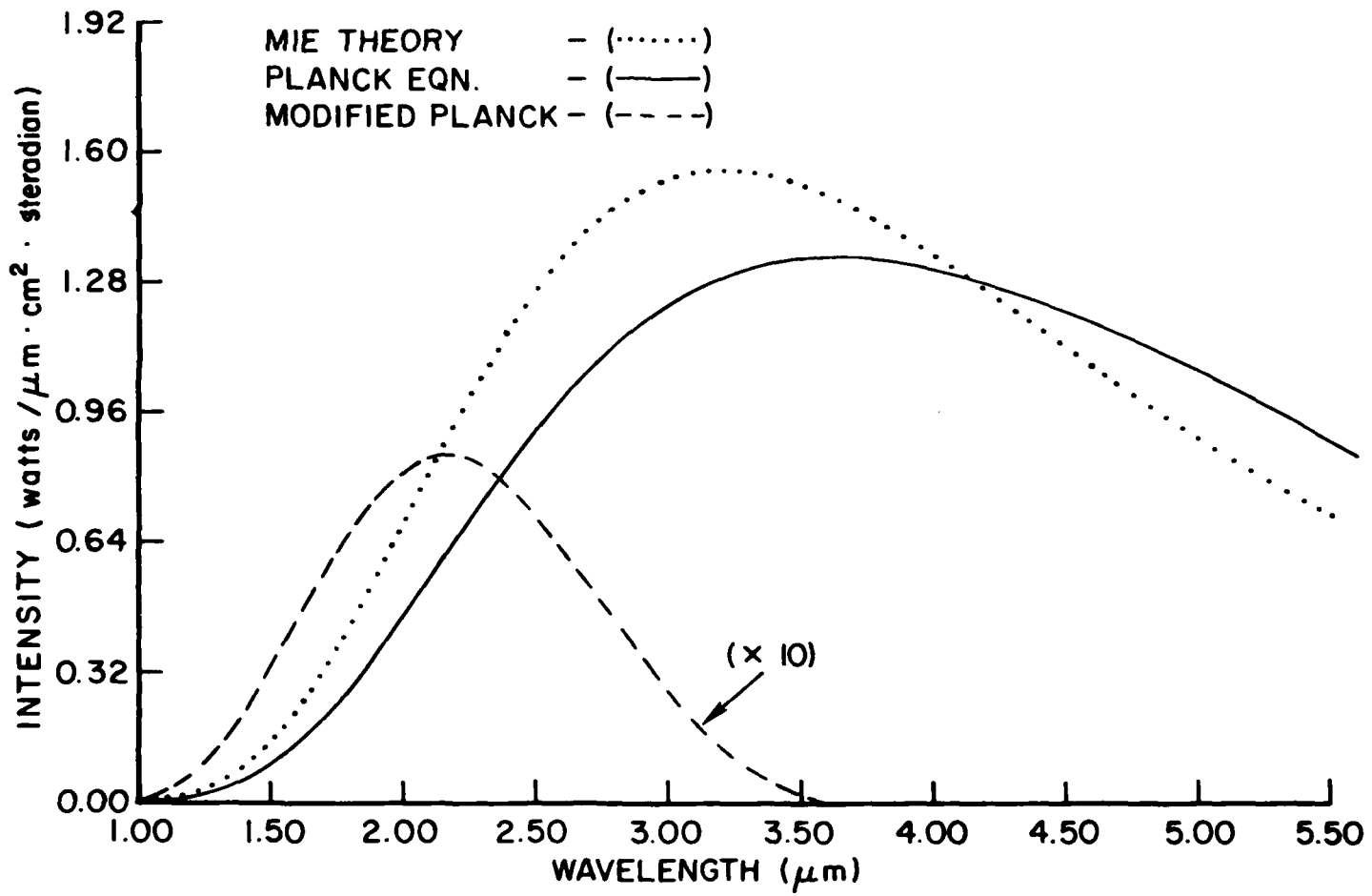

Figure 11. Calculated Spectra of Infrared Emission from: a Blackbody (Solid Curve), Particles Using Mie Theory (Dotted Curve), and Particles Using the Modified Planck Equation (Dashed Curve Multiplied by 10 to Graph on the Same Scale). Particle size distribution is shown in Figure 4, computed at 800 K.

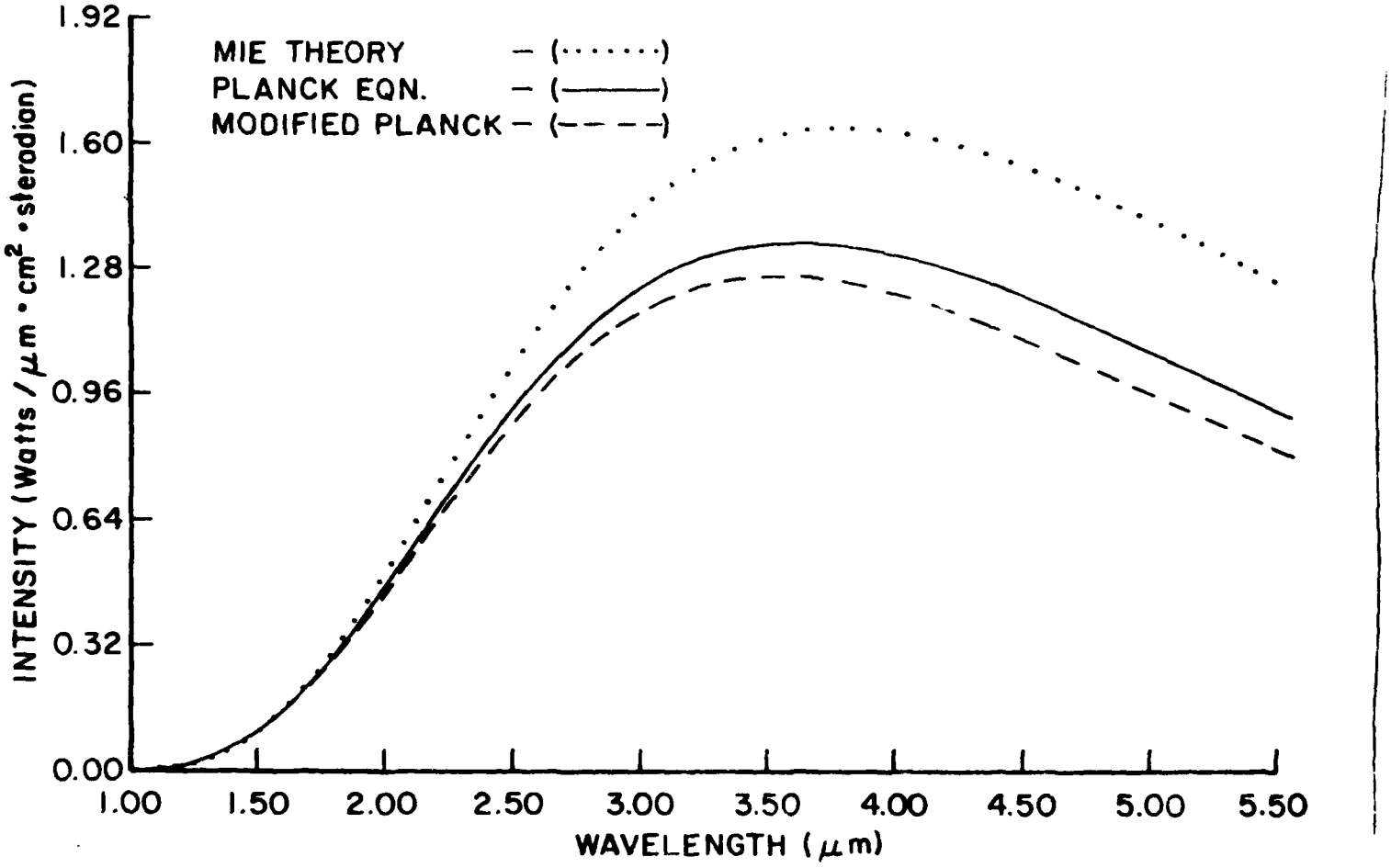

Figure 12. Calculated Spectra of Infrared Emission from: a Blackbody (Solid Curve), Particles Using Mie Theory (Dotted Curve), and Particles Using the Modified Planck Equation (Dashed Curve). Particle size distribution is shown in Table 1, computed at 800 K.

its number frequency in the size distribution. The reason the modified Planck formulation predicted a much lower intensity in Figure 11 is now easily seen. For the very small particle sizes shown in Figure 4, the factor $\{1-\lambda^2/2\pi^2d^2\}$ in Eq. (18) diminishes or completely cuts off any contribution to the total radiation for more than 90 percent (by number) of the particles at wavelengths of 2.5 μm and larger. Therefore, compared to Eq. (19), the total radiation intensity will be substantially less for the same particle sample. As the particle size becomes larger, however, this factor becomes less important, and as seen in Figure 12, the modified Planck formulation predicts a similar peak intensity for the large particle size distribution given in Table I.

3.2 EXPERIMENTAL RESULTS

Several sets of spectra were taken for each wavelength region. In each set the spectra were taken consecutively in time so that the experimental parameters of the run, flow velocity, temperature, and particle characteristics were held as constant as possible. The reduced data shown in Figure 13 are an example of a series of spectra taken consecutively showing the "shot-to-shot" reproducibility. These sets of spectra are then numerically averaged to reduce random noise. Averaged sets from the different wavelength regions are then matched on the basis of the measured flow temperature and slope at the point of juncture. Figure 14 is an example of composite data in which averaged spectra from different wavelength regions have been graphed on the same wavelength scale. For convenience in comparison, predictive calculations shown previously are included. The dotted curve is the Mie theory prediction while the dashed curve is the modified Planck equation curve. The two calculated curves have been normalized to the same height to match the data, and both calculations employ the same particle size distribution shown in Table I for a temperature of 820 K at which the data were taken. As predicted in Figure 12, the two calculated spectra are very similar. Both are in good agreement with the measured spectrum.

For a large particle size distribution, a distinction between the Mie theory approach and the modified Planck equation is difficult to achieve on

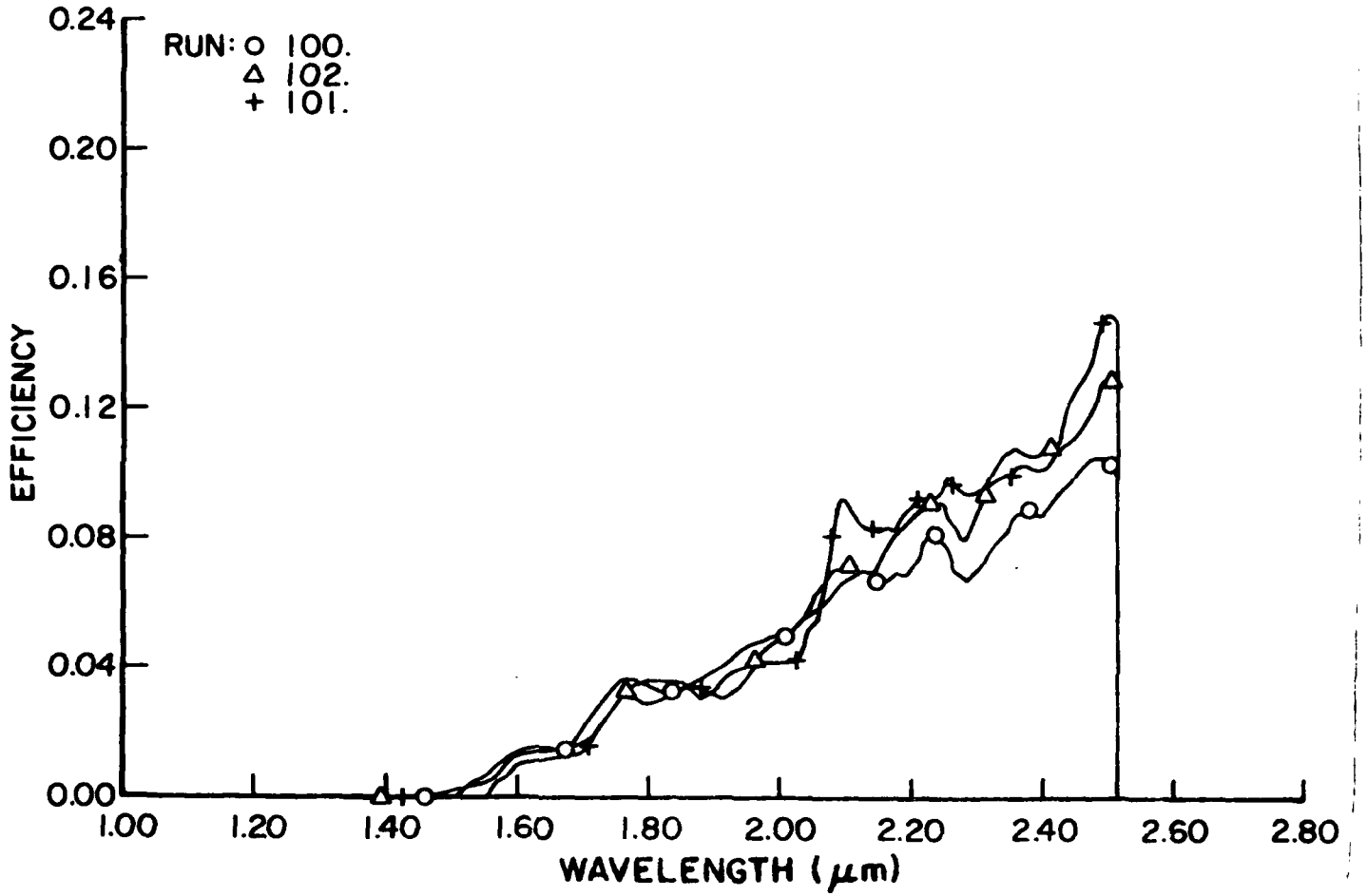

Figure 13. Set of Particle Radiation Spectra From 1.4 to 2.6 μm Wavelengths. Spectra were taken consecutively during a single run.

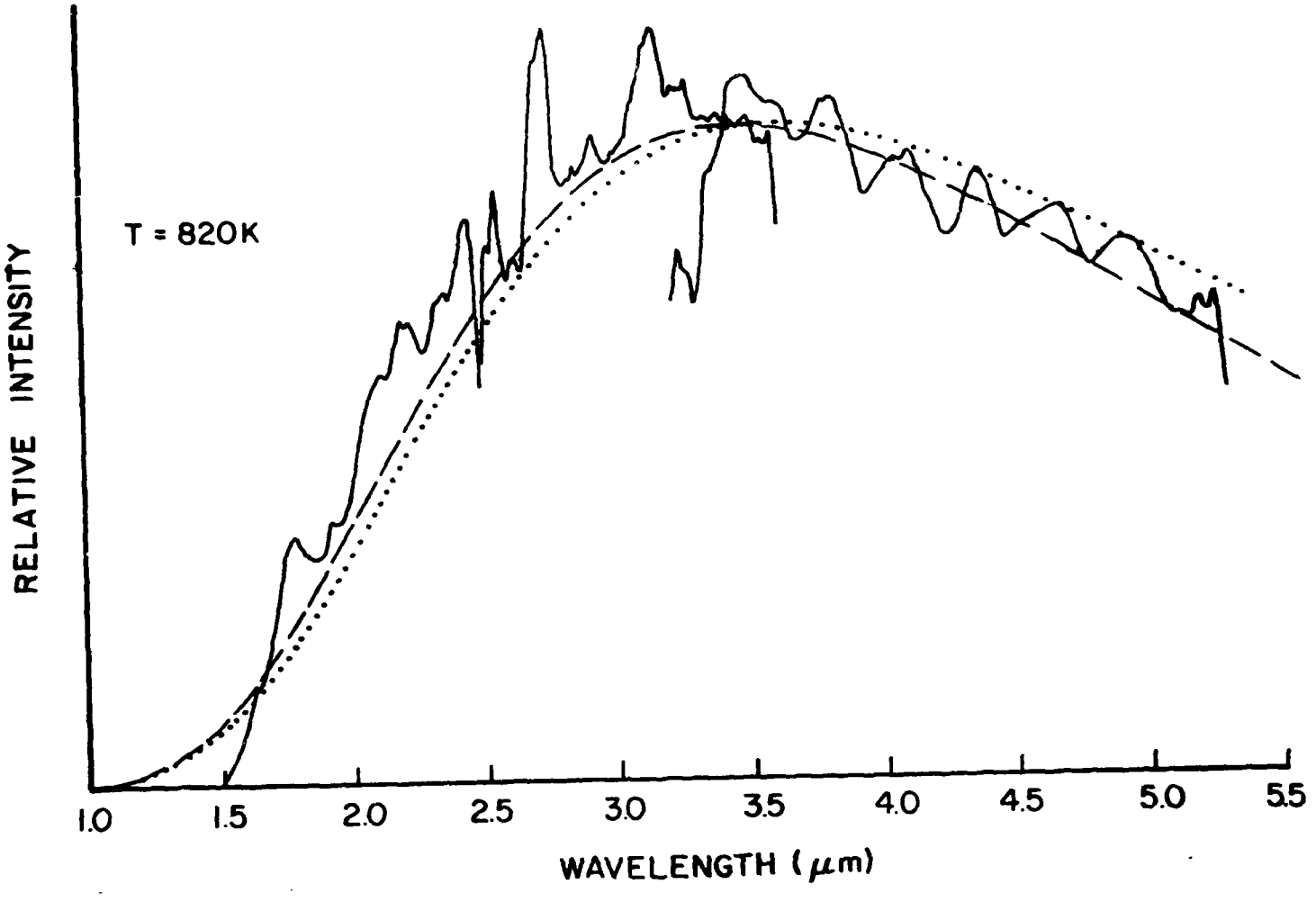

Figure 14. Composite Data Graphed on a Wavelength Axis. Calculated spectra have been overlaid in broken lines. The dashed curve is the modified Planck equation, and the dotted curve is the Mie theory result. Both calculations used the particle size distribution shown in Table I at the measured temperature of 820 K.

the basis of relative spectral shape, given the noise level of the data and the degree of error in the experimental parameters. Another possibility was differentiating the predictive formulations on the basis of absolute intensity of radiation. Since the optical system was calibrated against a standard blackbody source, it was possible to determine the absolute power levels of the infrared data from the particles as described below. Significant variation from different data sets is accounted for by differences in flow temperature and particle density. Nearly all the data sets yield peak intensity levels between 0.1 and 1.0 mW/μm. Since laser attenuation measurements were made during some of the experimental runs the quantity:

$$-\ln(I/I_o)/L = \sum_i N_i \sigma_i' \tag{21}$$

is easily determined, where I and I_o are the initial and attenuated laser beam intensities, L is the pathlength through the flow, and N_i and σ'_i are the number density and extinction cross section for particles of size i. From Eq. (21) it is straightforward to estimate the total geometric surface area (S) of all the particles present in the focal volume (V) of the scanning monochromator:

$$S = 4 \sum_i VN_i \sigma''_i = 2 \sum_i VN_i \sigma'_i \tag{22}$$

where σ''_i is the geometric cross section of the i^{th} size particle ($\sigma''_i = \pi r_i^2$), and from Mie theory, $\sigma'_i \approx 2\sigma''_i$. Using this surface area, the measured focal volume, and the subtended solid angle of the collection optics, the Mie theory approach predicts radiated intensities of around 0.1 mW/unit wavelength, for both the large and small size distributions. The modified Planck equation predicts values 20 times lower (see Figure 11) for the small size distribution, but values only about 25 percent lower for the large size distribution (see Figure 12). Consequently, both the Mie theory and modified Planck equation formulations predict radiation intensities for a large size distribution, which are within experimental error of the measured values.

This approach only provides a means of discrimination in the small particle size regime where differences in spectral shape should also be significant. Therefore, the immediate result is that the experimental data do not permit a clear distinction between the two theoretical formulations presented here due to the large (> 1.0 μm) average particle size in the two-phase flow.

3.3 ANALYSIS

Three basic parameters or experimental variables are essential to predictive calculations of thermal radiation from particulate material. They are size, emissivity (or index of refraction), and temperature. For the experiments described here, each of these variables was measured independently to generate the calculated spectra which generally agree with the observed radiation spectra. The question now considered is this. Can any information about these variables be derived from the observed spectra for situations where prior knowledge is not easily obtained? More simply, what is the diagnostic value of the thermal emission? This question can be explored by using the theoretical calculations which were seen to be consistent with the data. Figure 15 shows the dependence of the thermal emission from 0.5, 1.0, 2.0, and 4.0 μm diameter carbon particles at a temperature of 800 K using the formulation based on Mie theory. These spectra for different single size particles have all been normalized to approximately the same height to show the relative spectral distributions. Differences in absolute radiation intensities were less than a factor of two. From Figure 15, it is suggested that particles larger than about a micrometer in diameter have very similar spectra. Indeed, for applications where the emitted wavelength is larger than or equivalent to the particle diameter, this result is even independent of the theoretical formulation, since the transition to a macroscopic object is being made and the radiated spectrum is dominated by the Planck equation. Therefore, the size parameter appears to be relatively unimportant for applications involving larger sizes of particles at high temperatures.

The next parameter examined is the emissivity, or in the Mie theory formulation, the index of refraction of the particulate material. The important aspect here is the interdependence of the optical properties of materials with the particle size. While this is a fundamental question, subject to much

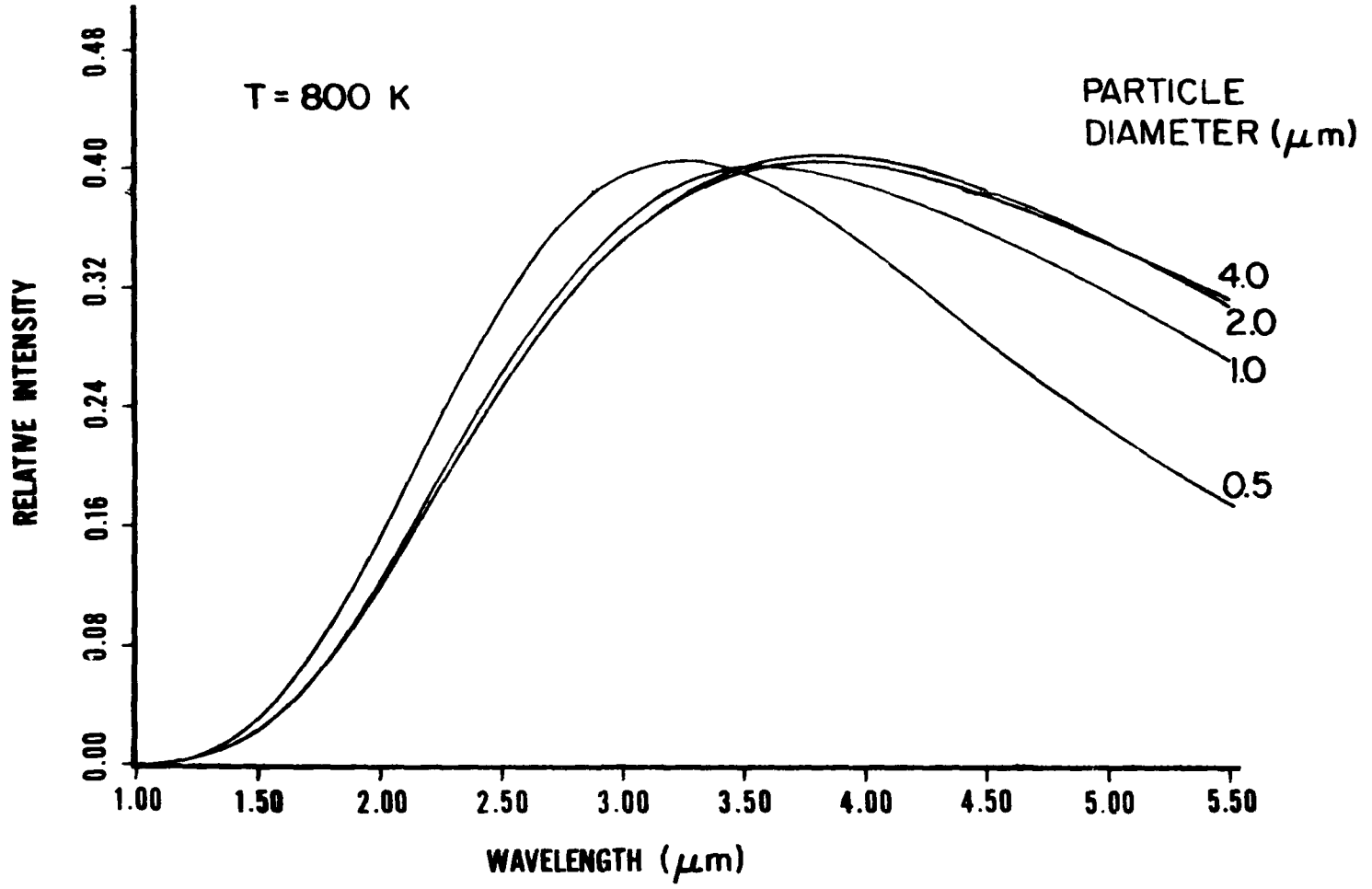

Figure 15. Calculated Spectra Using Mie Theory for Single Particles with Diameters of 0.5, 1.0, 2.0, and 4.0 μm.

interest and active investigation, the data collected for carbon particles suggests that no dramatic changes occur in the index of refraction for particle sizes on the order of 2 μm. Figure 16 displays calculated spectra (using Mie theory) for a single particle size of 2.0 μm, using values of 1.0, 1.7, and 3.0 for the real part of the index of refraction. (The imaginary part was -0.8.) The three spectra are graphed on an absolute scale and indicate that again relatively little effect is made by changing the index of refraction (real part) by factors of almost two. Similar changes in the imaginary part of the index of refraction had a much greater effect on the absolute intensity of radiation, but, when normalized, had negligible effect on the relative spectral distribution. Barring materials that have dramatically different optical constants (such as near zero imaginary parts of the index of refraction), and considering particles in the size range of a few micrometers or more, one could generalize these results to say that the thermal radiation spectral distribution is not a strong function of material composition.

The last parameter is the temperature of the two-phase flow. Figure 17 shows another composite graph of reduced data overlaid with three theoretical curves. The three spectra were calculated using the same particle size distribution (Table I), but at temperatures of 800, 850, and 900 K. The data themselves were recorded with the measured temperature in the two-phase flow of 840 ± 18 K. It can be seen that the theoretical curve of 850 K appears to be a best fit to the data, while the other two curves can be qualitatively rejected as marginal fits. This is an approximate way of establishing the accuracy with which the temperature can be derived from the data. In the absence of significant dependence on the other two parameters, size and index of refraction, the temperature can be "deduced" from the data within about ± 6 percent (50/850). This result invites speculation as to whether such spectra could provide temperature measurements in applications such as rocket plumes. Figure 18 shows calculated spectra for a 2.0 μm carbon particle exactly as in Figure 17, but with the temperatures elevated to around 3,100 K. The graphs in Figure 18 suggest that with similar signal-to-noise ratios, the thermal radiation from a two-phase flow could provide measurement of these elevated temperatures with better than 10 percent accuracy.

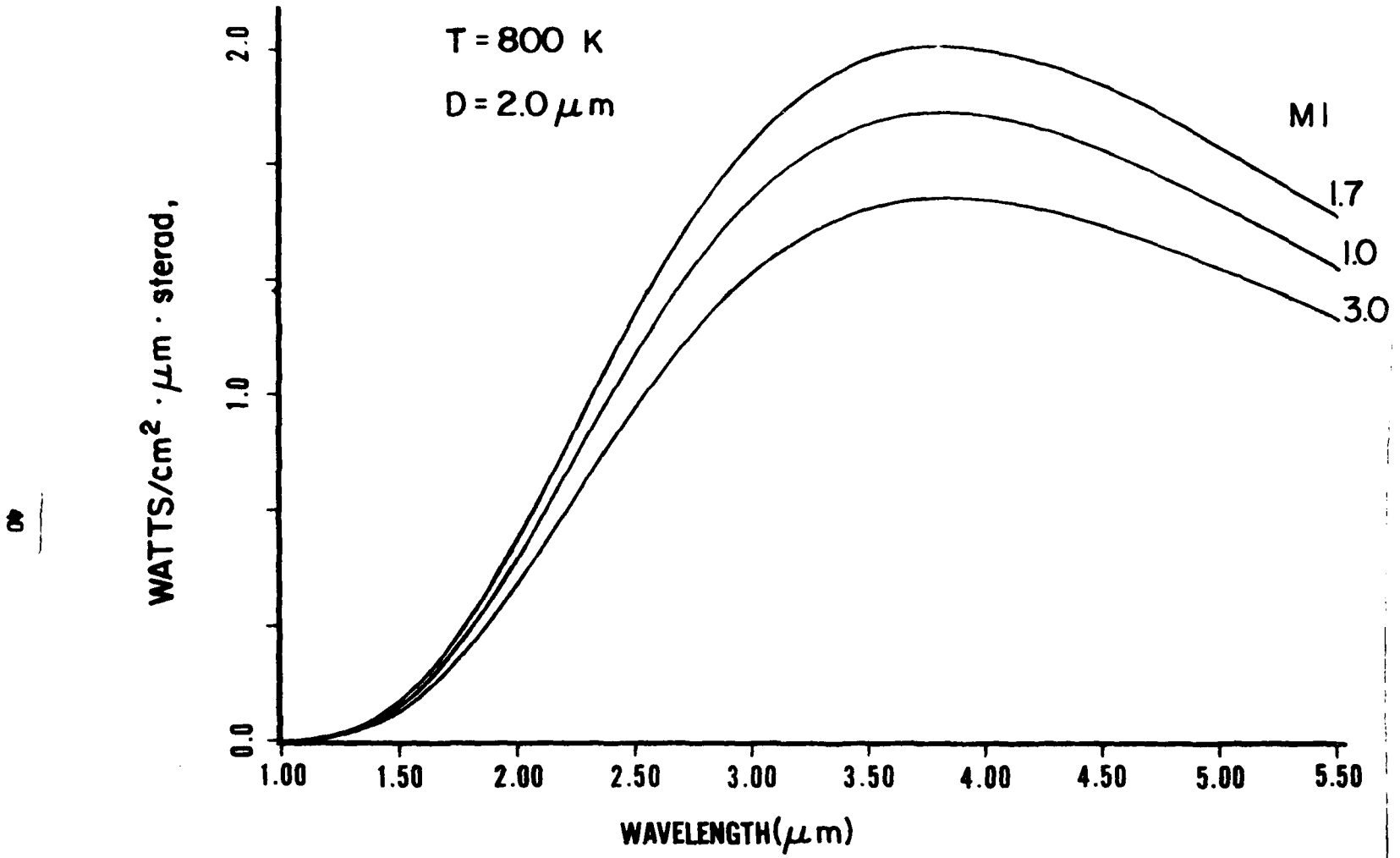

Figure 16. Calculated Spectra Using Mie Theory for a Single Particle of Diameter 2.0 μm with Values of 1.0, 1.7, and 3.0 for the Real Part of the Index of Refraction (MI). Spectra are plotted on an absolute scale with the imaginary part of the index refraction constant.

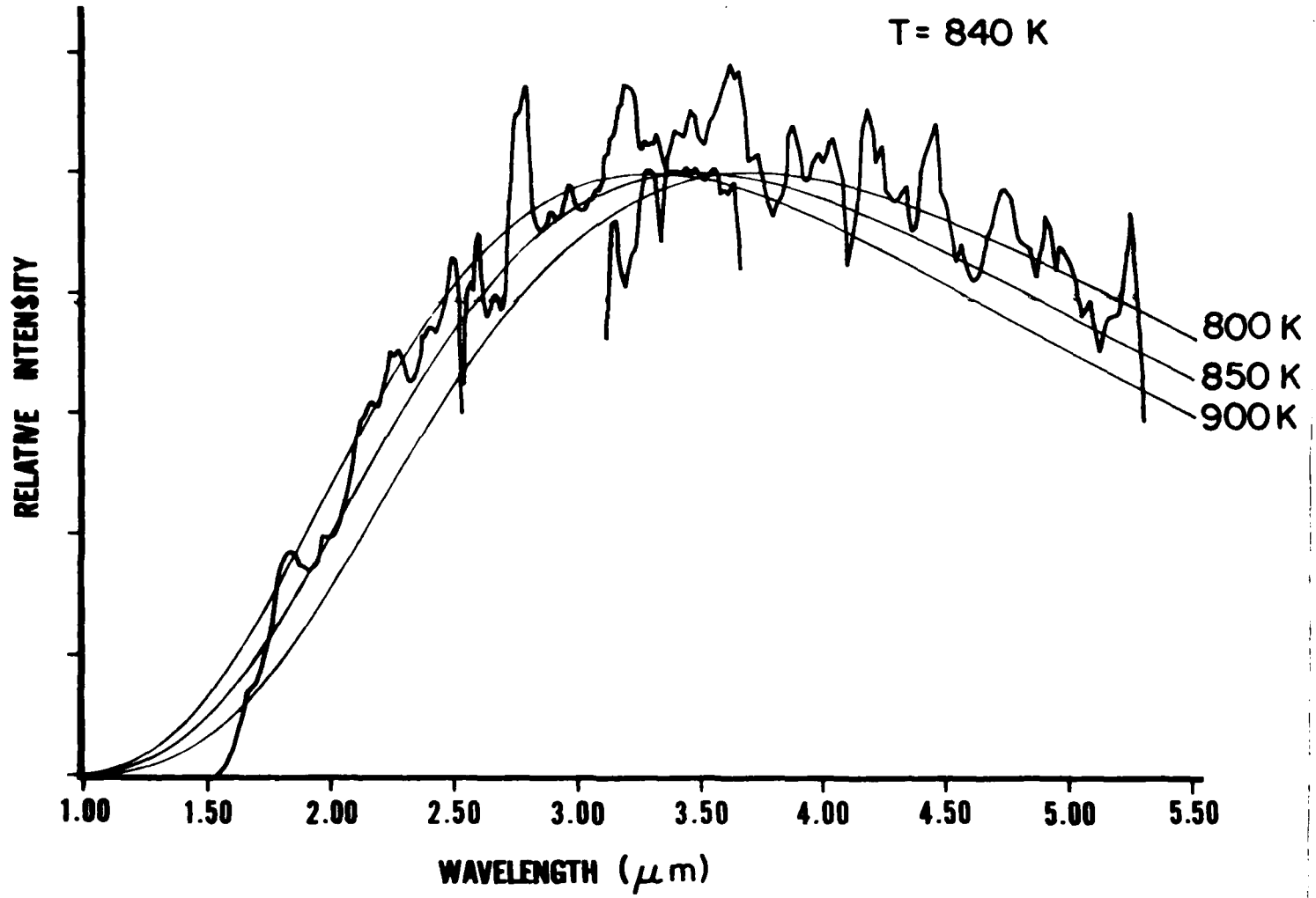

Figure 17. Composite Data Graphed on a Single Wavelength Axis Compared to Three Calculated Spectra Using Mie Theory. The temperature of the data is 840 K, while the calculations were made for 800, 850, and 900 K. Calculations used the particle size distribution shown in Table 1.

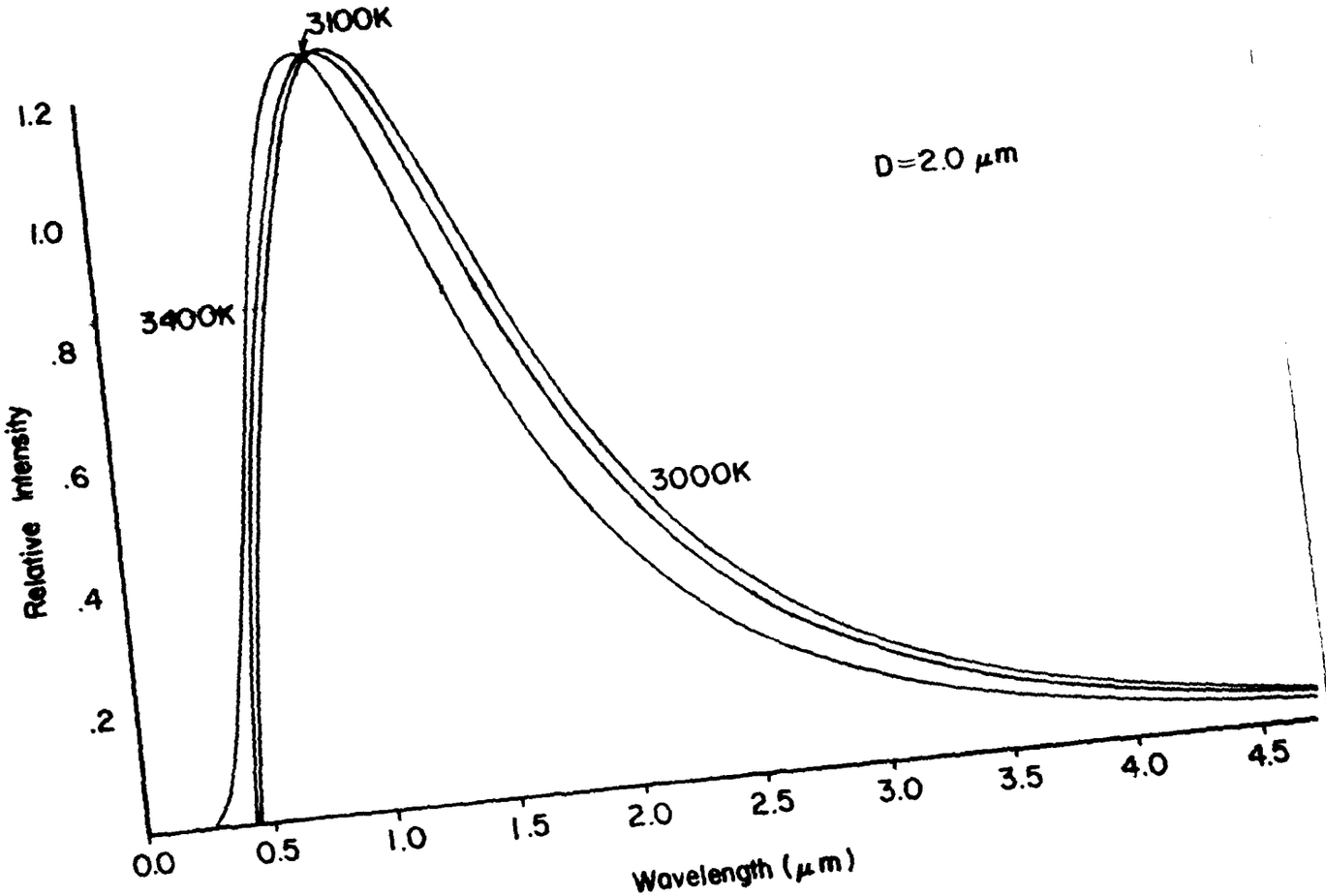

Figure 16. Calculated Spectra Using Mie Theory for a Single 2.0 μm Diameter Carbon Particle for Three Different Temperatures: 3,000, 3,100, and 3,400 K.

SECTION 4

CONCLUSIONS

In terms of the ultimate applications of this work, it appears that the two fundamental theoretical approaches for determining particle emissivities are not a crucial factor in predicting infrared emission as long as the conditions of large particles size (> 1 μm), and high temperatures (> 800 K) are met. In this regime theoretical calculations of the thermal radiation will be dominated by the Planck equation for a large range of particle sizes and a large range of materials. This further implies that the measurement of infrared emission may be used as a diagnostic probe for the temperature of the flow. For particular application to rocket exhausts, calculations indicated that at higher temperatures (3000 K) an accuracy of ± 10% or better may be achieved. These results were obtained from, and therefore are directly applicable only to two-phase flows which are optically thin. Complications due to radiative transfer have not been considered. In ultimate application to optically thick flows this last consideration together with large spatial gradients may be the limiting factors.